Electronic Supplementary Information

for the manuscript entitled

Lanthanide-based metallogels with tunable luminescence: Nanomolar detection of a nerve agent simulant and anticounterfeiting applications

Aashish, Ruchika Gupta, Hina Goyal, Rajeev Gupta*

Department of Chemistry, University of Delhi, Delhi–110007

Experimental section

Materials and methods

All chemicals and reagents were procured from commercial sources and were used without further purification. The solvents were purified utilizing the standard literature methods.[1] The precursor **L'** was synthesized according to our earlier report.[2]

Syntheses

Synthesis of L'' and L1

$H_2L^{p\text{-}COOEt}$-O-$(CH_2)_{17}CH_3$ (L''). **L'** (1.00 g, 2.09 mmol) and 1-bromooctadecane (0.83 g, 2.51 mmol) were dissolved in 20 mL DMF followed by the addition of solid K_2CO_3 (0.57 g, 4.18 mmol). The reaction mixture was stirred for 6 h at 60 °C. The unreacted K_2CO_3 was filtered off from the reaction mixture, and the solvent was removed under the reduced pressure. The product was isolated after washing with diethyl ether. Yield: 1.33 g (88 %). ^{1}H NMR spectrum (400 MHz, DMSO-d_6) δ 8.04 (d, J = 8.7 Hz, 4H), 7.98 (d, J = 8.9 Hz, 4H), 7.82 (s, 2H), 4.30 (q, J = 7.1 Hz, 4H), 4.25 (t, J = 6.5 Hz, 2H), 1.84 – 1.70 (m, 2H), 1.47 – 1.39 (m, 2H), 1.32 (t, J = 7.1 Hz, 6H), 1.28 – 1.12 (m, 28H), 0.81 (t, J = 6.9 Hz, 3H). FTIR spectrum (Zn–Se, selected peaks, ν/cm^{-1}): 3364 (N–H), 2916 (C–H), 1705 ($COOCH_2CH_3$), 1588 (C=O). Elemental analysis for $C_{43}H_{59}N_3O_7$: C, 70.75; H, 8.15; N, 5.76. Found: C, 70.82; H, 8.20; N, 5.82.

$H_2L^{p\text{-}COOH}$-O-$(CH_2)_{17}CH_3$ (L1). The ligand **L1** was obtained after the base-assisted hydrolysis of **L''**. **L''** (0.5 g, 0.68 mmol) was dissolved in a mixture of THF-H_2O (3:1, v/v) and treated with 5 equiv. of NaOH (0.13 g, 3.4 mmol). This reaction mixture was stirred for 12 h at room temperature. To this reaction mixture, an aqueous solution of 4N HCl was added until pH reached 3.0-4.0. The resulting solution was vacuum evaporated to remove THF, which led to the precipitation of a product that was isolated, washed with water, and air-dried. Yield: 0.36 g (80 %). ^{1}H NMR spectrum (400 MHz, DMSO-d_6) δ 11.15 (s, 2H), 8.04 (d, J = 8.6 Hz, 4H), 7.98 (d, J = 8.6 Hz, 4H), 7.80 (s, 2H), 4.20 (t, J = 5.7 Hz, 2H), 1.80 – 1.64 (m, 2H), 1.46 – 1.31 (m, 2H), 1.32 – 1.11 (m, 28H), 0.78 (t, J = 6.6 Hz, 3H). ^{13}C NMR spectrum (100 MHz, DMSO-d_6) δ 167.97, 167.43, 162.20, 151.10, 142.46, 130.75, 126.91, 120.52, 111.99, 69.26, 31.76, 29.51, 29.46, 29.38, 29.19, 29.09, 25.70, 22.55, 14.37. FTIR spectrum (Zn–Se, selected peaks, ν/cm^{-1}): 3269 (N–H), 2913 (C–H), 1685 (COOH), 1587 (C=O). Elemental analysis for $C_{39}H_{51}N_3O_7$: C, 69.52; H, 7.63; N, 6.24. Found: C, 69.70; H, 7.69; N, 6.26.

Synthesis of L''' and L2

$H_2L^{p\text{-}COOEt}$-O-$(CH_2)_4$-CH_3 (L'''). **L'''** was synthesized using a similar procedure as mentioned for **L''**, however, using the following reagents: **L'** (1.00 g, 2.09 mmol), pentyl bromide (0.37 g, 2.51 mmol), and K_2CO_3 (0.57g, 4.18 mmol). Yield: 1.00 g (88 %). ^{1}H NMR spectrum (400 MHz, DMSO-d_6) δ 11.34 (s, 2H), 8.06 (d, J = 8.6 Hz, 4H), 7.97 (d, J = 8.5 Hz, 4H), 7.78 (s, 2H), 4.28 (q, J = 7.0 Hz, 4H), 4.21 (t, J = 5.8 Hz, 2H), 1.83 – 1.67 (m, 2H), 1.47 – 1.32 (m, 4H), 1.30 (t, J = 7.1 Hz, 6H), 0.87 (t, J = 7.1 Hz, 3H). FTIR spectrum (selected peaks, ν/cm^{-1}): 3244 (N–H), 2918 (C–H), 1710 ($COOCH_2CH_3$), 1585 (C=O). Elemental analysis calculated for $C_{30}H_{33}N_3O_7$: C, 65.80; H, 6.07; N, 7.67. Found: C, 65.85; H, 6.12; N, 7.65.

$H_2L^{p\text{-}COOH}$-O-$(CH_2)_4$-CH_3 (L2). Ligand **L2** was synthesized using a procedure similar to that mentioned for **L1**; however, using **L'''**. Yield: 0.36 g (82 %). ^{1}H NMR spectrum (400 MHz, DMSO-d_6) δ 12.86 (s, 2H), 11.20 (s, 2H), 8.09 (d, J = 7.9 Hz, 4H), 8.03 (d, J = 7.9 Hz, 4H), 7.85 (s, 2H), 4.26 (t, J = 6.4 Hz, 2H), 1.85 – 1.70 (m, 2H), 1.54 – 1.30 (m, 4H), 0.92 (t, J = 5.8 Hz, 3H). ^{13}C NMR spectrum (100 MHz, DMSO-d_6) δ 167.98, 167.42, 162.31, 151.11, 142.53, 130.80, 126.68, 120.57, 112.02, 69.29, 28.38, 27.93, 22.31, 14.35. FTIR spectrum (selected peaks, ν/cm^{-1}): 3266 (N–H), 2961 (C–H), 1682 (COOH), 1592 (C=O). Elemental analysis calculated for $C_{26}H_{25}N_3O_7$: C, 63.54; H, 5.13; N, 8.55. Found: C, 63.62; H, 5.15; N, 8.58.

Synthesis of L'''' and L3

$H_2L^{p\text{-}COOEt}$-O-$(CH_2)_9$-CH_3 (L''''). **L''''** was synthesized using a similar procedure as mentioned for **L''**; however, using the following reagents: **L'** (1.00 g, 2.09 mmol), decyl bromide (0.55 g, 2.51 mmol) and K_2CO_3 (0.57g, 4.18 mmol). Yield: 1.18 g (92 %). ^{1}H NMR spectrum (400 MHz, DMSO-d_6) δ 11.33 (s, 2H), 8.07 (d, J = 8.6 Hz, 4H), 8.00 (d, J = 8.7 Hz, 4H), 7.77 (s, 2H), 4.27 (q, J = 7.2 Hz, 4H), 4.18 (t, J = 6.6 Hz, 2H), 1.77 – 1.65 (m, 2H), 1.42 – 1.34 (m, 2H), 1.24 – 1.12 (m, 12H), 1.29 (t, J = 7.0 Hz, 6H), 0.80 (t, J = 5.6 Hz, 3H). FTIR spectrum (selected peaks, ν/cm^{-1}): 3259 (N–H), 2916 (C–H), 1705 ($COOCH_2CH_3$), 1585 (C=O). Elemental analysis calculated for $C_{35}H_{43}N_3O_7$: C, 68.05; H, 7.02; N, 6.80. Found: C, 67.96; H, 6.95; N, 6.87.

$H_2L^{p\text{-}COOH}$-O-$(CH_2)_9$-CH_3 (L3). Ligand **L3** was synthesized using a procedure similar to that mentioned for **L1**; however, using **L''''**. Yield: 0.38 g (85 %). ^{1}H NMR spectrum (400 MHz, DMSO-d_6) δ 12.86 (s, 2H), 11.19 (s, 2H), 8.09 (d, J = 7.6 Hz, 4H), 8.03 (d, J = 8.0 Hz, 4H), 7.82 (s, 2H), 4.23 (t, J = 6.4 Hz, 2H), 1.81 – 1.69 (m, 2H), 1.46 – 1.35 (m, 2H), 1.35 – 1.16 (m, 12H), 0.85 (t, J = 5.7 Hz, 3H). ^{13}C NMR spectrum (100 MHz, DMSO-d_6) δ 167.96, 167.42,

162.21, 151.05, 142.48, 130.78, 126.80, 120.61, 111.99, 69.28, 31.77, 29.45, 29.42, 29.18, 28.66, 25.74, 22.57, 14.41. FTIR spectrum (selected peaks, ν/cm^{-1}): 3244 (N–H), 2931 (C–H), 1682 (COOH), 1585 (C=O). Elemental analysis calculated for $C_{31}H_{35}N_3O_7$: C, 66.30; H, 6.28; N, 7.48. Found: C, 66.42; H, 6.19; N, 7.49.

Synthesis of L'''' and L4

$H_2L^{p\text{-}COOEt}$-O-$(CH_2)_{21}CH_3$ (L''''). **L''''** was synthesized using a similar procedure as mentioned for **L''**; however, using the following reagents: **L'** (1.00 g, 2.09 mmol), 1-bromodocosane (0.97 g, 2.51 mmol) and K_2CO_3 (0.57 g, 4.18 mmol). Yield: 1.39 g (85 %). ^{1}H NMR spectrum (400 MHz, DMSO-d_6) δ 8.04 (d, J = 8.8 Hz, 4H), 7.97 (d, J = 8.8 Hz, 4H), 7.81 (s, 2H), 4.29 (q, J = 7.1 Hz, 4H), 4.24 (t, J = 6.5 Hz, 2H), 1.79 – 1.73 (m, 2H), 1.45 – 1.36 (m, 2H), 1.33 (t, J = 7.1 Hz, 6H), 1.24 – 1.14 (m, 36H), 0.82 (t, J = 5.7 Hz, 3H). FTIR spectrum (Zn–Se, selected peaks, ν/cm^{-1}): 3355 (N–H), 2920 (C–H), 1710 ($COOCH_2CH_3$), 1587 (C=O). Elemental analysis for $C_{47}H_{67}N_3O_7$: C, 71.82; H, 8.59; N, 5.35. Found: C, 71.85; H, 8.53; N, 5.39.

$H_2L^{p\text{-}COOH}$-O-$(CH_2)_{21}CH_3$ (L4). Ligand **L4** was synthesized using a procedure similar to that mentioned for **L1**; however, using **L''''**. Yield: 0.37 g (80 %). ^{1}H NMR spectrum (400 MHz, DMSO-d_6) δ 10.97 (s, 2H), 8.00 (d, J = 8.6 Hz, 4H), 7.92 (d, J = 8.6 Hz, 4H), 7.82 (s, 2H), 4.26 (t, J = 5.7 Hz, 2H), 1.88 – 1.68 (m, 2H), 1.52 – 1.38 (m, 2H), 1.24 – 1.15 (m, 36H), 0.83 (t, J = 6.8 Hz, 3H). FTIR spectrum (Zn–Se, selected peaks, ν/cm^{-1}): 3268 (N–H), 2918 (C–H), 1688 (COOH), 1582 (C=O). Elemental analysis for $C_{43}H_{59}N_3O_7$: C, 70.75; H, 8.15; N, 5.76. Found: C, 70.72; H, 8.12; N, 5.80.

Physical measurements

The FTIR spectra were recorded using an Agilent Cary 630 spectrometer with a diamond ATR. NMR spectral measurements were done with a Jeol 400 MHz spectrometer. Elemental analysis was performed using an Elementar Analysen Systeme GmbH Vario EL-III instrument. Powder X-ray diffraction (PXRD) patterns were obtained with a Rigaku Table-Top XRD or a Bruker AXS D8 Discover instrument (Cu Kα radiation, λ = 1.54184 Å). The samples were ground and subjected to a range of θ = 5–60° at a slow scan rate at room temperature. Fluorescence spectral studies were performed with a Cary Eclipse fluorescence spectrometer. The solid-state photoluminescence studies and lifetime measurements were performed using a Quanta master up-conversion and down-conversion fluorimeter (QM-8450-11) equipped with a 450W Xe source lamp and a 980 nm laser. FESEM, EDAX, and elemental dot mapping analyses were

carried out with a Zeiss GeminiSEM 500 instrument. The rheological measurements were carried out with an Anton Paar Rheometer (MCR-302) equipped with stainless steel parallel plates (20 mm diameter).

X-ray diffraction studies

Single crystal X-ray diffraction data for **L1** and **L3** were collected on a Rigaku Oxford XtaLAB Synergy-DW diffractometer equipped with a graphite monochromatic MoKα radiation (λ = 0.71073 Å).[3] SMART[4] was used for collecting frames of data, indexing reflections and determining the lattice parameters; SAINT[4] for integration of the intensity of reflections and scaling; and SADABS[5] for absorption correction. The frames were collected at 293(2) K. The structures were solved by the direct methods using SIR-97[6] and refined by the full-matrix least-squares refinement techniques on F^2 using SHELXL-97[7] incorporated in the Olex2 crystallographic package.[8] All calculations and structure refinements were performed using the Olex2 program. The hydrogen atoms were fixed at the calculated positions using the isotropic thermal parameters, whereas non-hydrogen atoms were refined anisotropically. Both **L1** and **L3** always produced poorly diffracting thin crystals, most probably due to the disordered attached alkyl chains. Although a few efforts resulted in data collection and structure solutions, poor data convergence only allowed partial structure solutions.

Crystal data for **L1**: cell = triclinic, space group = *P*-1, a = 6.0822(6), b = 14.6083(13), c = 27.503(2), α = 75.093(8)°, β = 86.011(7)°, γ = 80.145(8)°, V = 2325.7(4), Z = 2.

Crystal data for **L3**: cell = triclinic, space group = *P*-1, a = 7.4183(6), b = 14.6850(5), c = 15.6692(5), α = 90.631(3)°, β = 96.020(5)°, γ = 102.567(6)°, V = 1655.88(16), Z = 2.

Fluorescence spectral measurements

For sensing studies, 1 mg samples of **L1-Eu** and **L1-Tb** xerogels were dispersed in 4 mL of EtOH, followed by 30 min of sonication. All stock solutions of analytes (2.5 mM) adenosine triphosphate (ATP), adenosine diphosphate (ADP), adenosine monophosphate (AMP), Na_3PO_4, Na_2HPO_4, NaH_2PO_4, H_3PO_4, and mustard gas simulants, dimethyl methylphosphate (DMMP), diethyl chlorophosphate (DCP), diethyl cyanophosphate (DECP), CH_3COCl, and $SOCl_2$ were prepared in EtOH. All fluorescence spectral experiments were performed with a 1.0 cm path length cuvette at 25±1 °C in EtOH.

Determination of Stern-Volmer (K_{SV}) and binding (K_b) constants

Stern-Volmer constants (K_{SV}) were calculated using the Stern-Volmer equation (1), where I_0 and I are the emission intensities of **L1-Eu** or **L1-Tb** xerogels in the absence and presence of DMMP used as a quencher (Q), respectively.[9,10] The binding constants (K_b) were computed using the Benesi-Hildebrand equation (2),[11] where I is the emission intensity of **L1-Eu** or **L1-Tb** xerogels in the presence of [DMMP] at 618 and 546 nm, respectively; I_0 is the intensity of **L1-Eu** or **L1-Tb** xerogels in the absence of [DMMP]; and I_{min} is the minimum fluorescence intensity in the presence of [DMMP]. K_b was obtained by a ratio of intercept and slope in $1/(I-I_0)$ vs. 1/[DMMP] plot.

$$I_0/I = 1 + K_{SV}[\text{DMMP}] \quad (1)$$

$$1/(I-I_0) = 1/\{K_b(I_0-I_{min})[\text{DMMP}]\} + 1/(I_0-I_{min}) \quad (2)$$

Determination of detection limit

The detection limits were calculated using the equation (3), where k is the slope of a plot of fluorescence intensity of **L1-Eu** or **L1-Tb** xerogels vs DMMP concentration and σ is the standard deviation of ten blank fluorescence measurements of **L1-Eu** or **L1-Tb** xerogels.[12]

$$\text{Detection limit} = 3\sigma/k \quad (3)$$

Inclusion studies

A 30 mg sample of **L1-Eu** or **L1-Tb** xerogel was suspended in MeCN and impregnated with 5 equiv. of DMMP for 12 h at 25 °C. The impregnated sample was filtered, washed thrice with fresh MeCN, and dried under vacuum. This sample was used for the characterization.

References

1. D. D. Perrin, W. L. F. Armarego, D. R. Perin, Purification of Laboratory Chemicals, Pergamon Press: Oxford, UK, 1980.
2. Aashish, R. Gupta and R. Gupta, *Sens. Diagn.*, 2023, **2**, 1585–1596.
3. CrysAlisPro, v. 1.171.33.49b; Oxford Diffraction Ltd., 2009.
4. SMART & SAINT Software Reference Manual, Version 6.45; Bruker Analytical X-Ray Systems, Inc., Madison, 2003.
5. G. M. Sheldrick, SADABS, A software for empirical absorption correction, Ver. 2.05; University of Göttingen: Göttingen, Germany, 2002.
6. A. Altomare, G. Cascarano, C. Giacovazzo, A. Guagliardi, M. C. Burla, G. Polidori and M. Camalli, *J. Appl. Crystallogr.*, 1994, **27**, 435–435.
7. G. M. Sheldrick, A short history of SHELX. *Acta Crystallogr. A*, 2008, **64**, 112–122.
8. O. V. Dolomanov, L. J. Bourhis, R. J. Gildea, J. A. K. Howard and H. Puschmann, OLEX2: a complete structure solution, refinement and analysis program. *J. Appl. Crystallogr.*, 2009, **42**, 339–341.
9. P. Kumar, V. Kumar, S. Pandey and R. Gupta, *Dalton Trans.*, 2018, **47**, 9536–9545.
10. P. Kumar, V. Kumar and R. Gupta, *Dalton Trans.*, 2017, **46**, 10205–10209.
11. H. A. Benesi and J. H. Hildebrand, *J. Am. Chem. Soc.*, 1949, **71**, 2703–2707.
12. H. Goyal, S. Pachisia and R. Gupta, *Cryst. Growth Des.*, 2020, **20**, 6117–6128.

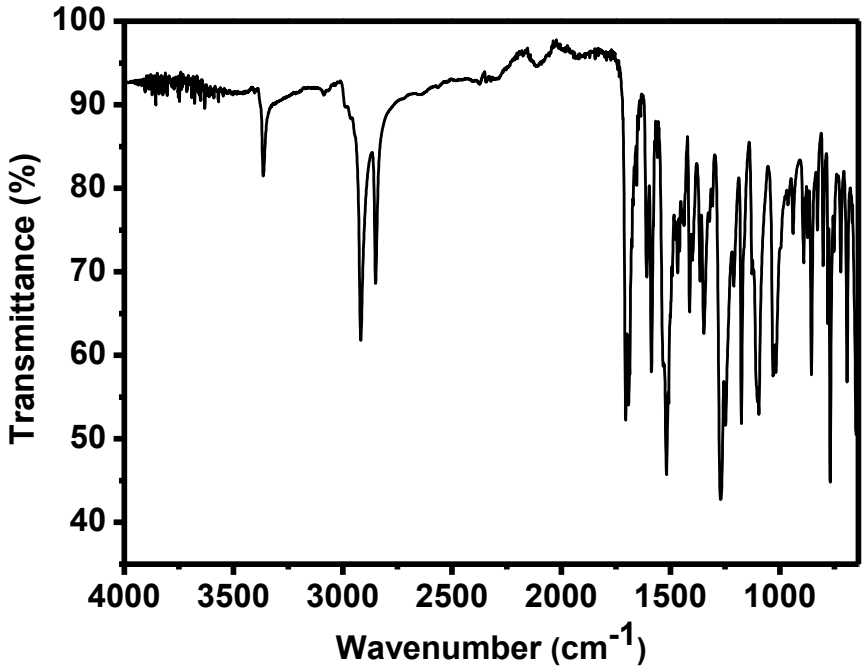

Figure S1. FTIR spectrum of **L''**.

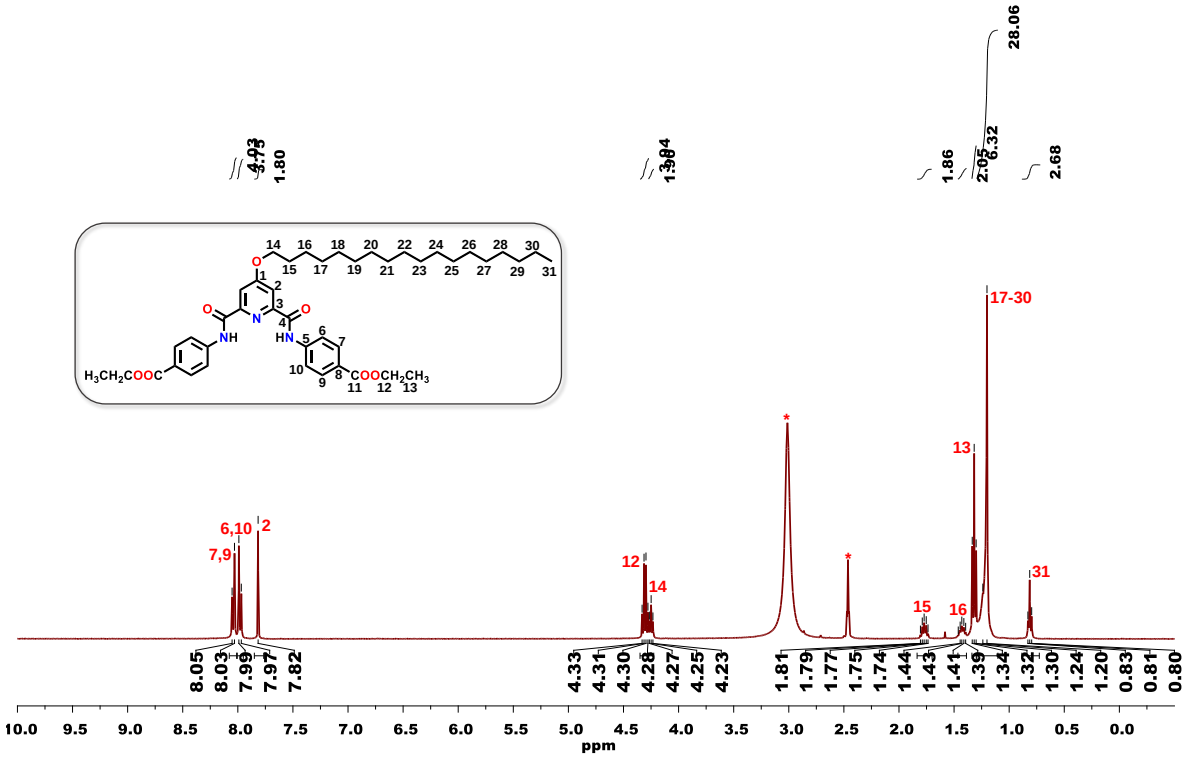

Figure S2. ^{1}H NMR spectrum of **L''** in DMSO-d_6 solvent where * represents the residual solvent and/or adventitious water peaks.

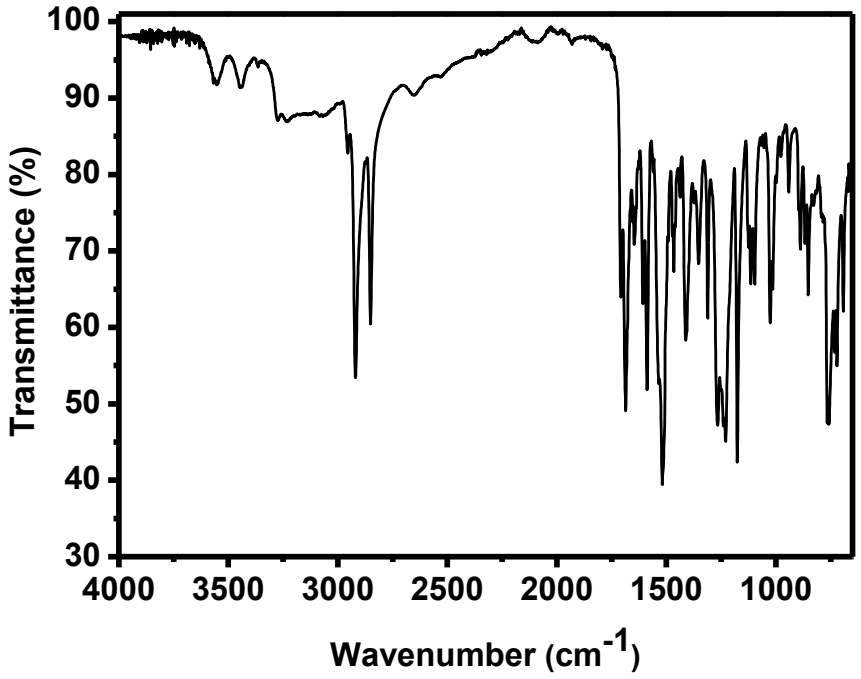

Figure S3. FTIR spectrum of ligand **L1**.

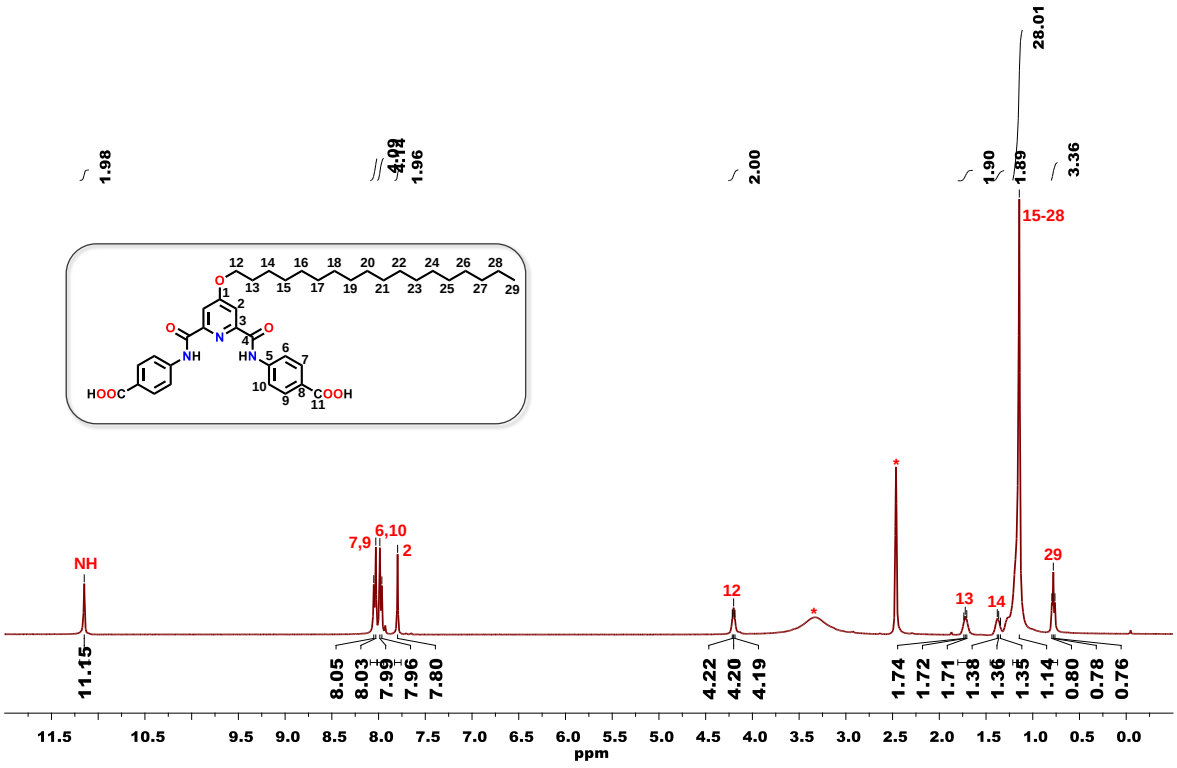

Figure S4. ^{1}H NMR spectrum of ligand **L1** in DMSO-d_6 solvent where * represents the residual solvent and/or adventitious water peaks.

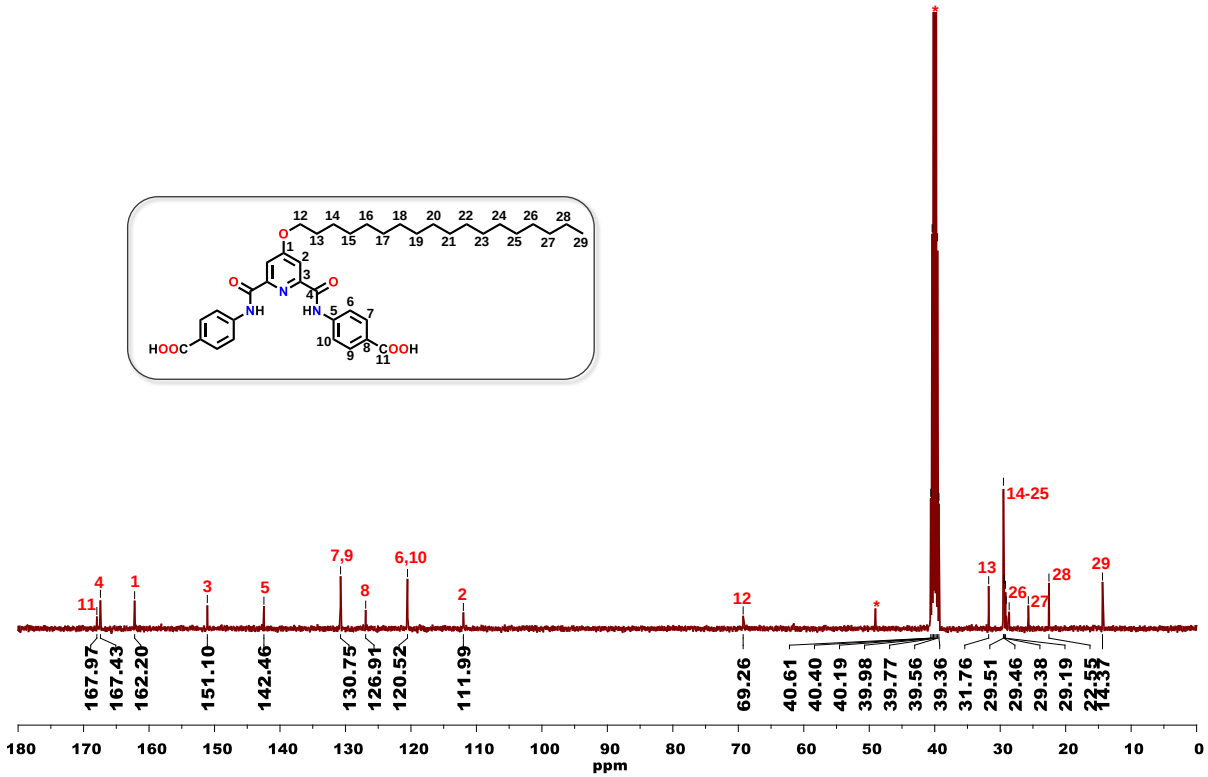

Figure S5. ^{13}C NMR spectrum of ligand **L1** in DMSO-d_6 solvent where * represents the residual solvent peak.

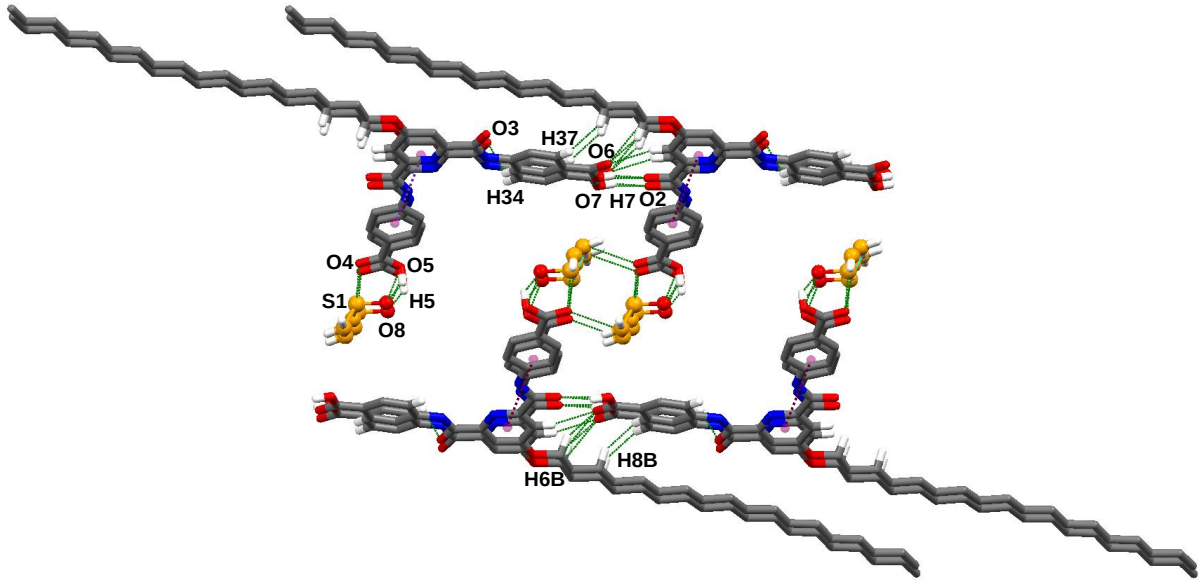

Figure S6. Crystal structure of ligand **L1** showing the packing of different molecules of **L1** and lattice DMSO molecules (ball and stick mode where C and O atoms are shown in gold and red, respectively) when viewed along *a*-axis.

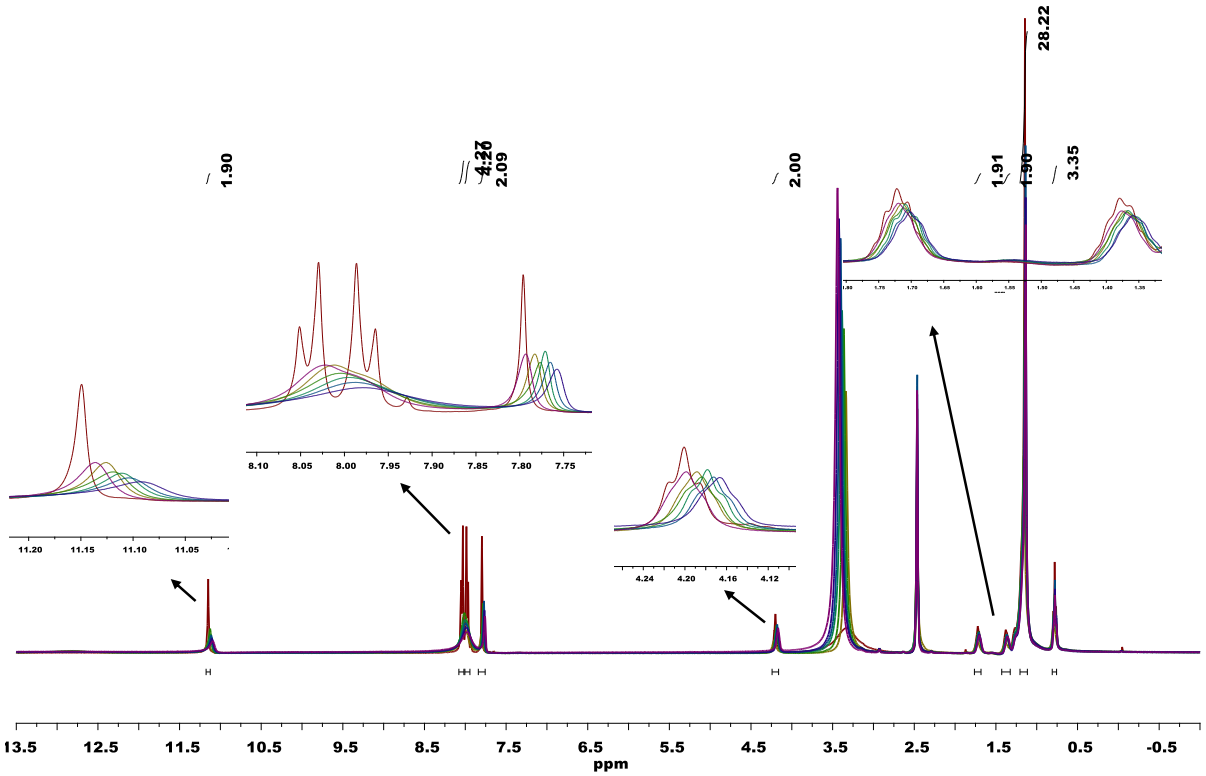

Figure S7. ^{1}H NMR spectral titration of ligand **L1** after the successive addition of up to three equiv. of the Eu^{3+} salt. Spectra were recorded in DMSO-d_6 solvent.

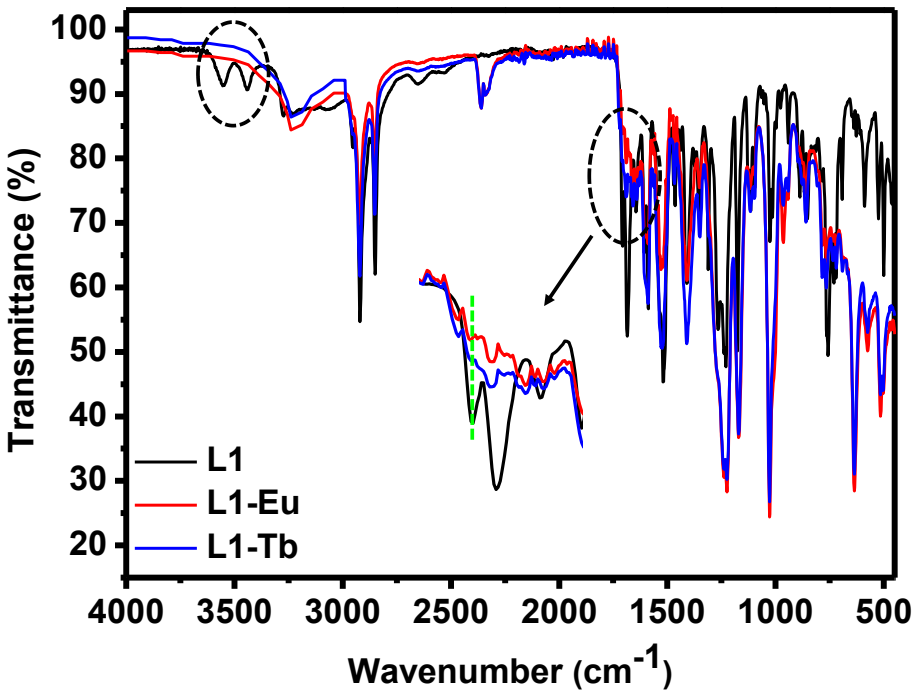

Figure S8. FTIR spectra of ligand **L1** (black trace), **L1-Eu** (red trace), and **L1-Tb** (blue trace).

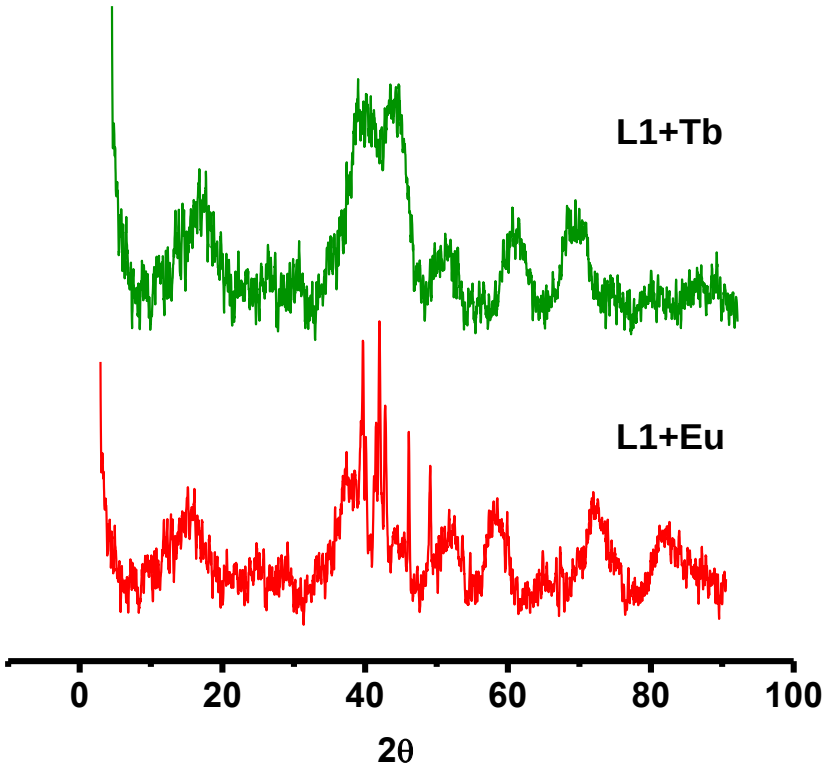

Figure S9. X-ray powder diffraction patterns for xerogels **L1-Eu** (red trace) and **L1-Tb** (green trace).

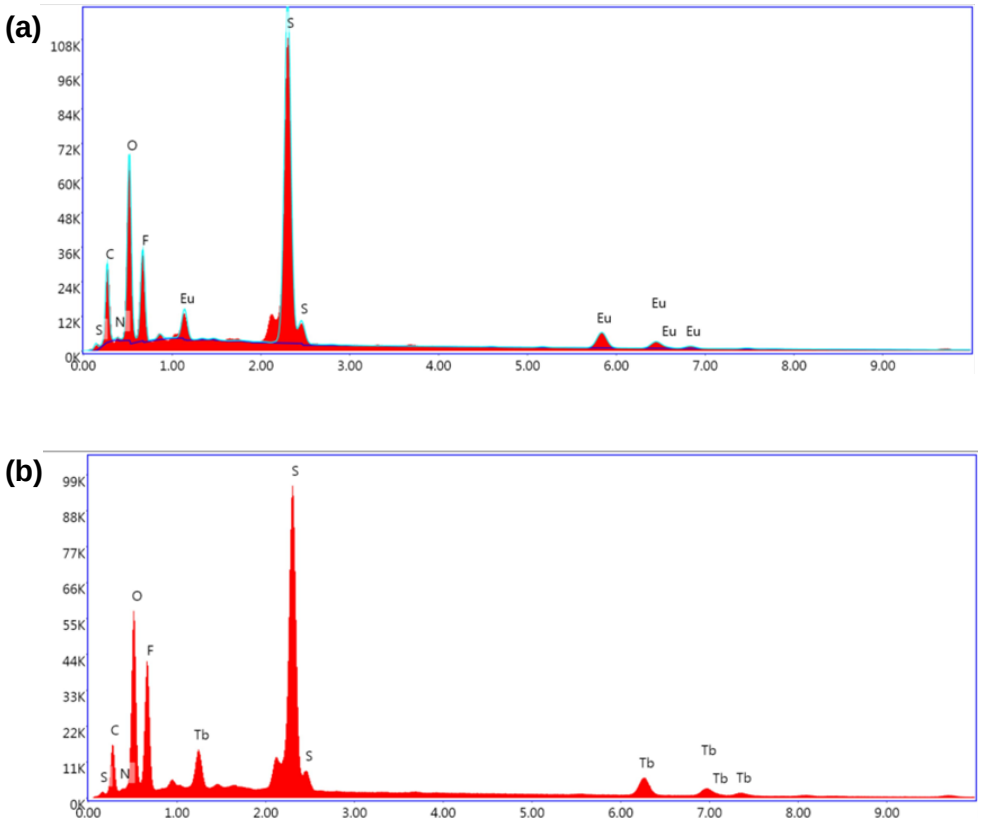

Figure S10. EDAX spectra for (a) **L1-Eu** and (b) **L1-Tb**.

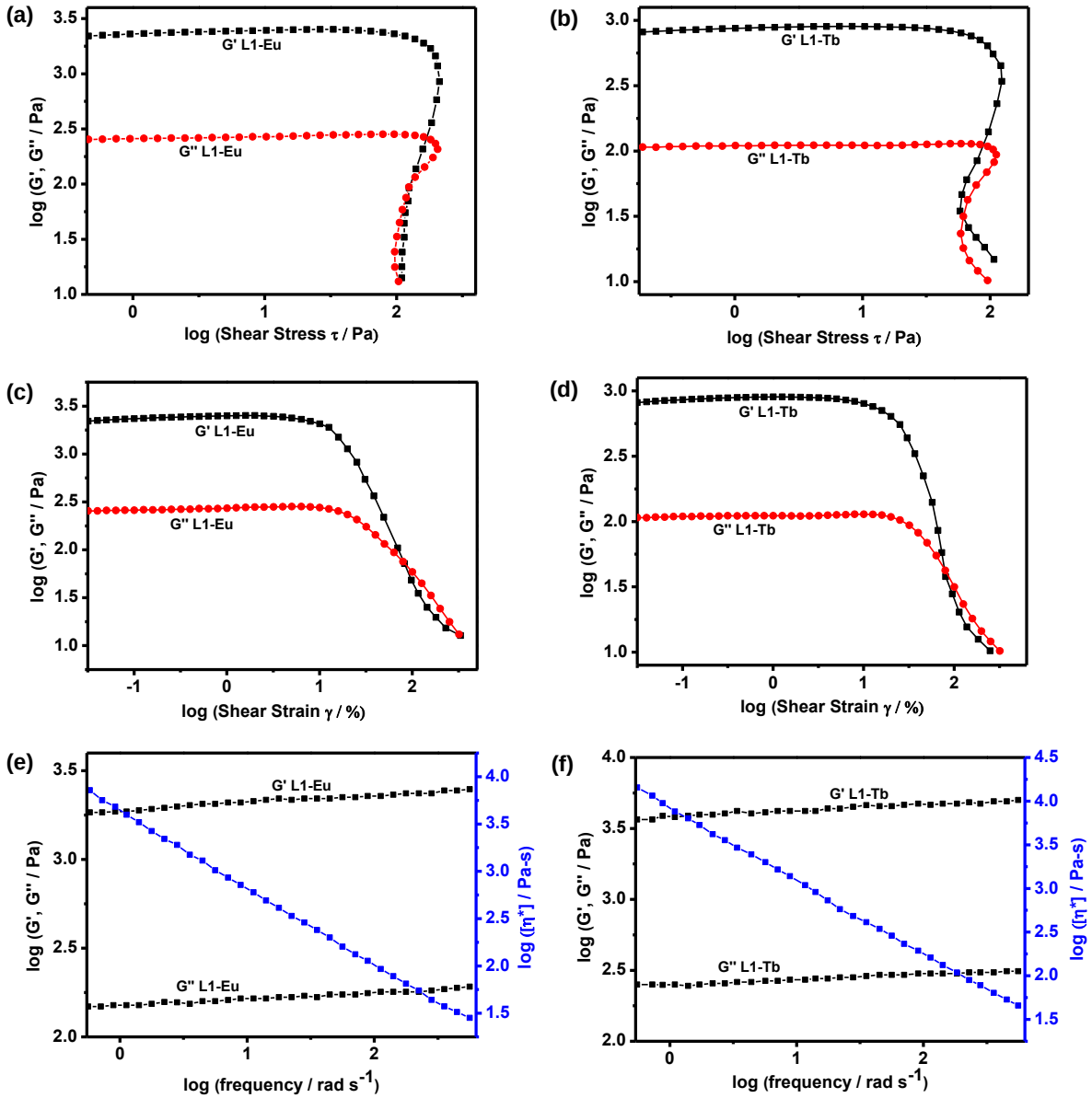

Figure S11. Rheological measurements for **L1-Eu** and **L1-Tb** gels. Dynamic stress sweep at constant frequency for (a) **L1-Eu** and (b) **L1-Tb**. Dynamic strain sweep at constant frequency for (c) **L1-Eu** and (d) **L1-Tb**. Dynamic frequency sweep at constant strain and secondary axis showing the complex viscosity for (e) **L1-Eu** and (f) **L1-Tb**.

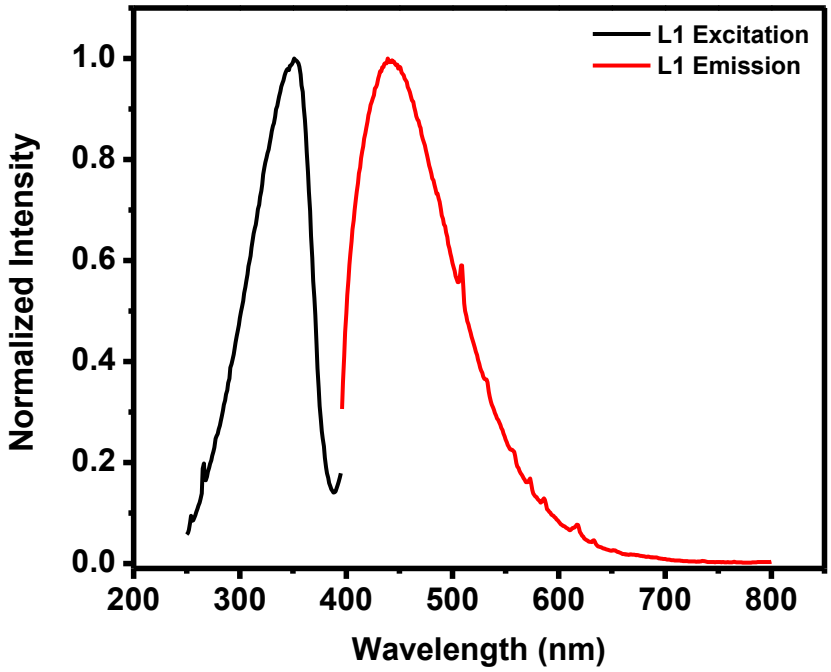

Figure S12. Excitation and emission spectra of **L1**.

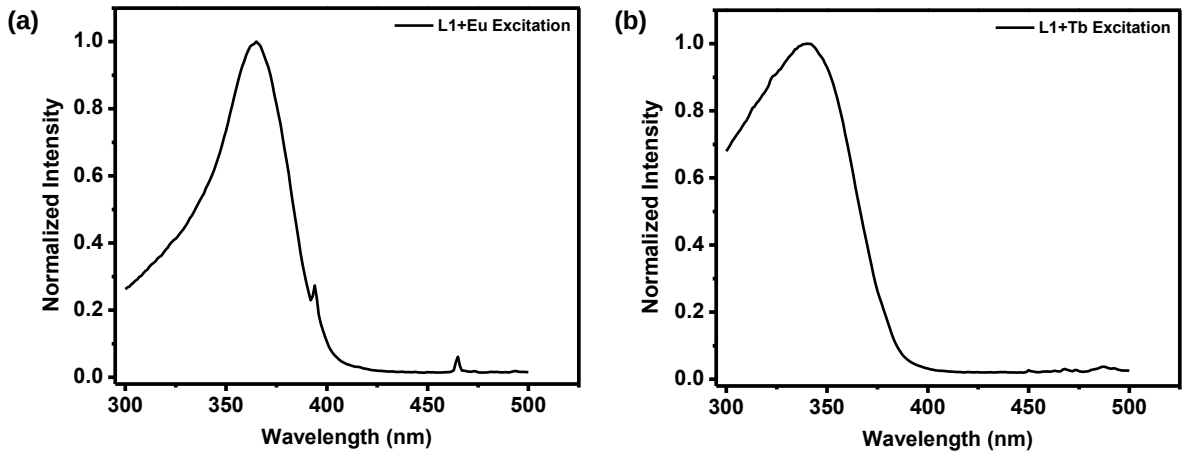

Figure S13. Excitation spectra for (a) **L1-Eu** and (b) **L1-Tb**.

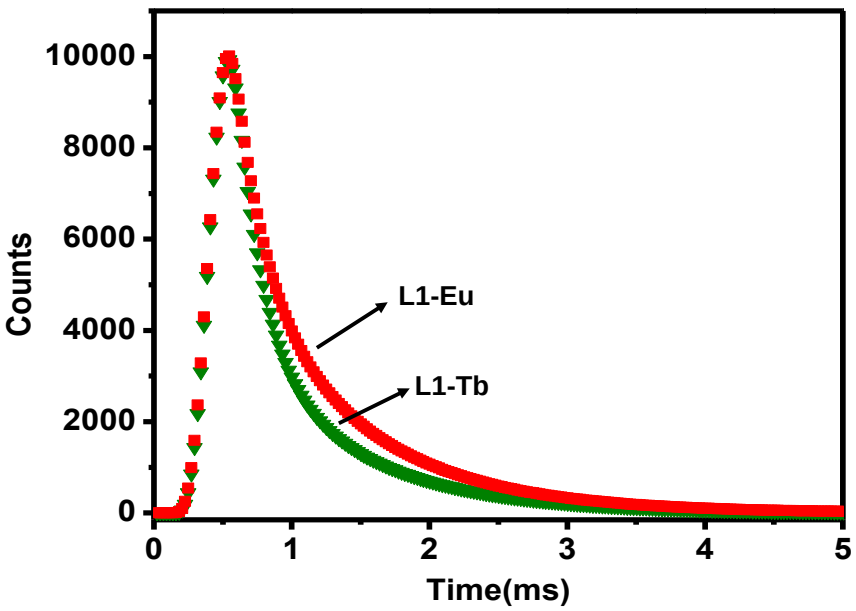

Figure S14. Lifetime decay profiles for **L1-Eu** (red squares) and **L1-Tb** (green triangles).

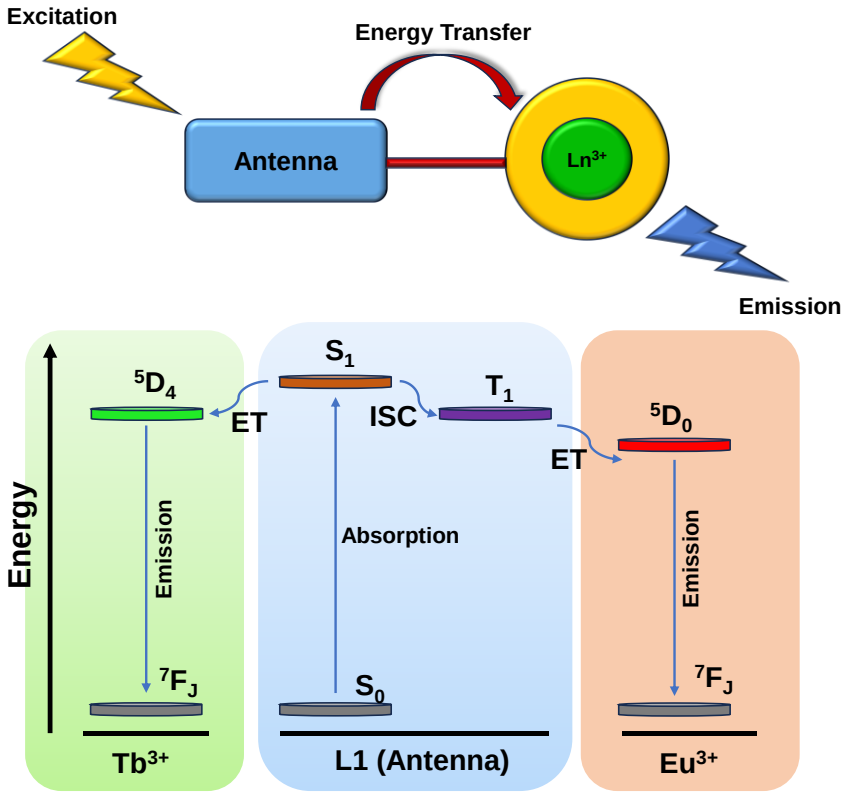

Figure S15. A schematic illustration of the "antenna effect" shown by the Ln-metallogels.

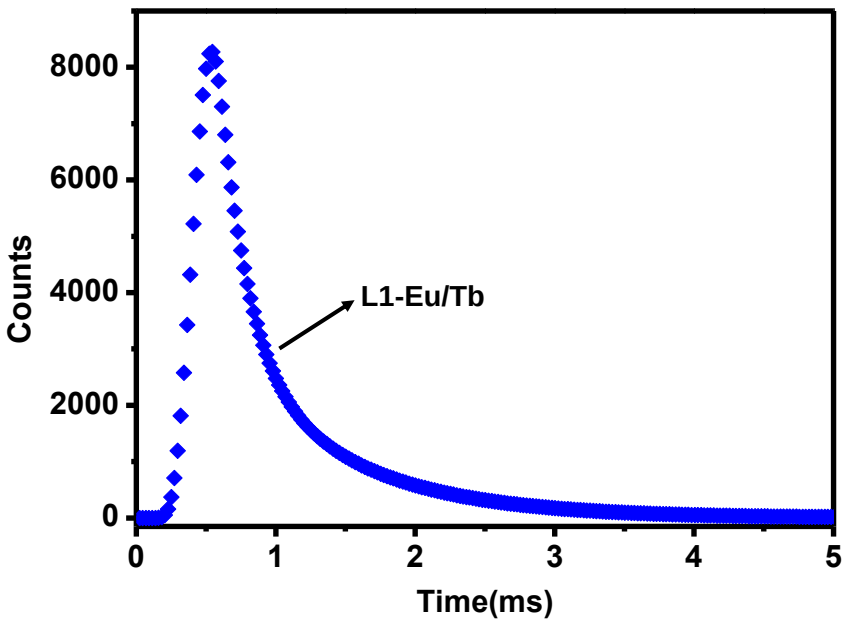

Figure S16. Lifetime decay profile for **L1-Eu/Tb**.

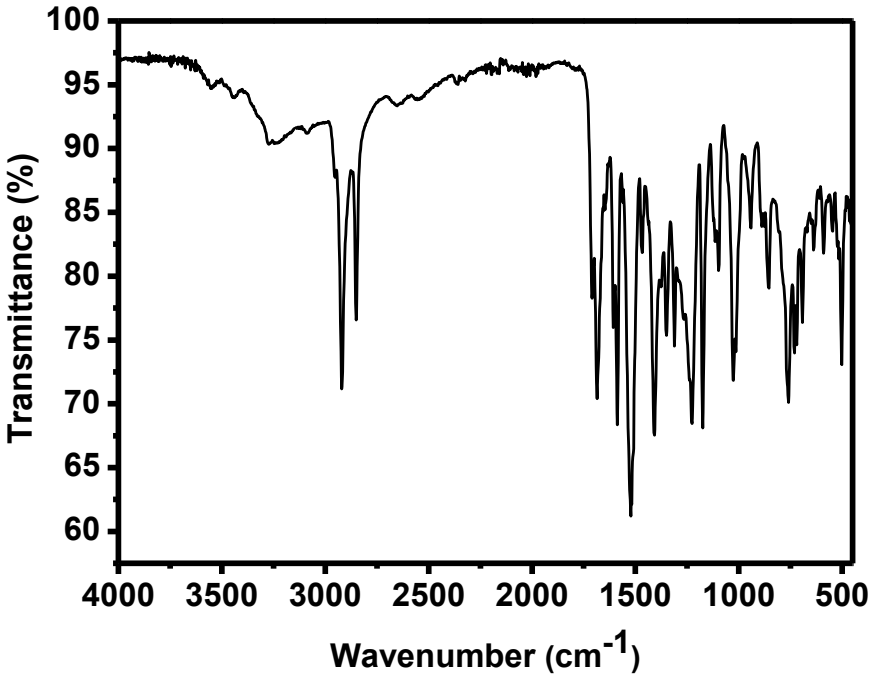

Figure S17. FTIR spectrum of **L1-Eu/Tb**.

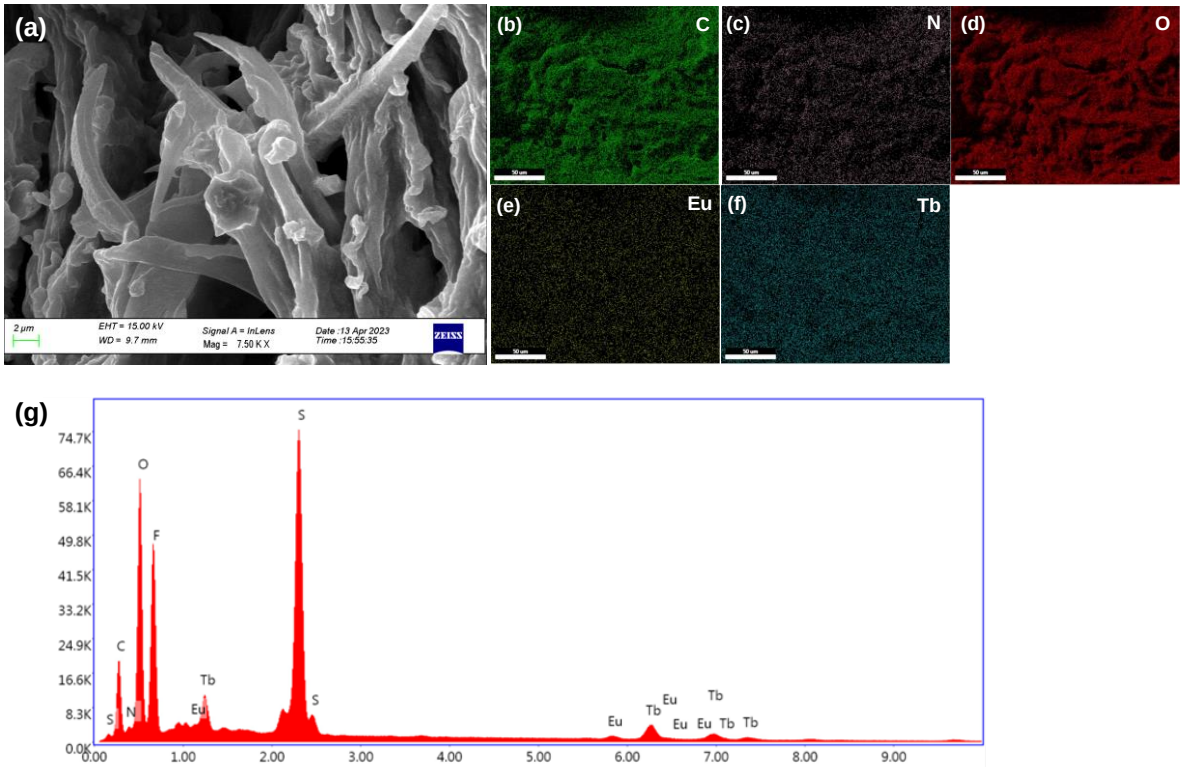

Figure S18. (a) FESEM image of **L1-Eu/Tb**, (b-f) elemental mapping analysis of **L1-Eu/Tb**, and (g) EDAX spectrum of **L1-Eu/Tb**.

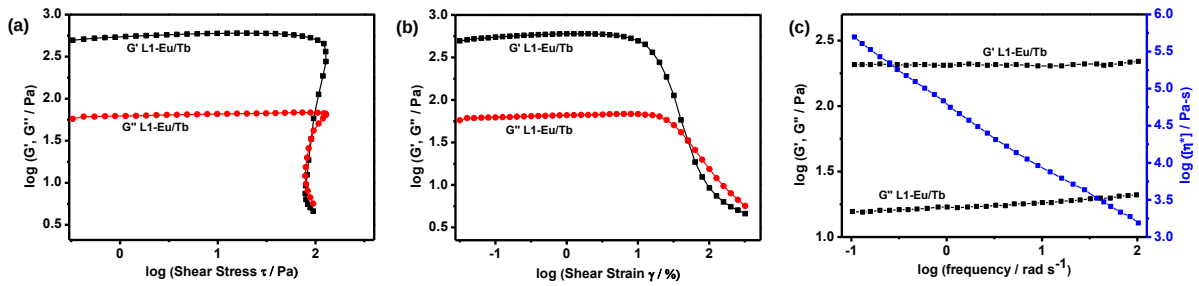

Figure S19. Rheological measurements for **L1-Eu/Tb**. (a) Dynamic stress sweep at constant frequency for **L1-Eu/Tb**, (b) dynamic strain sweep at constant frequency for **L1-Eu/Tb**, and (c) dynamic frequency sweep at constant strain and secondary axis showing the complex viscosity for **L1-Eu/Tb**.

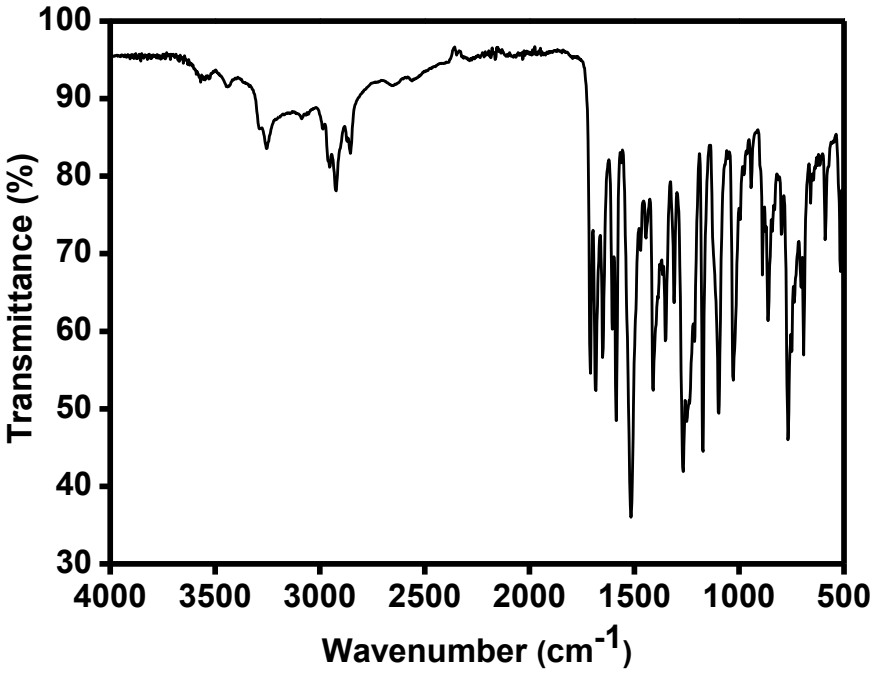

Figure S20. FTIR spectrum of **L'''**.

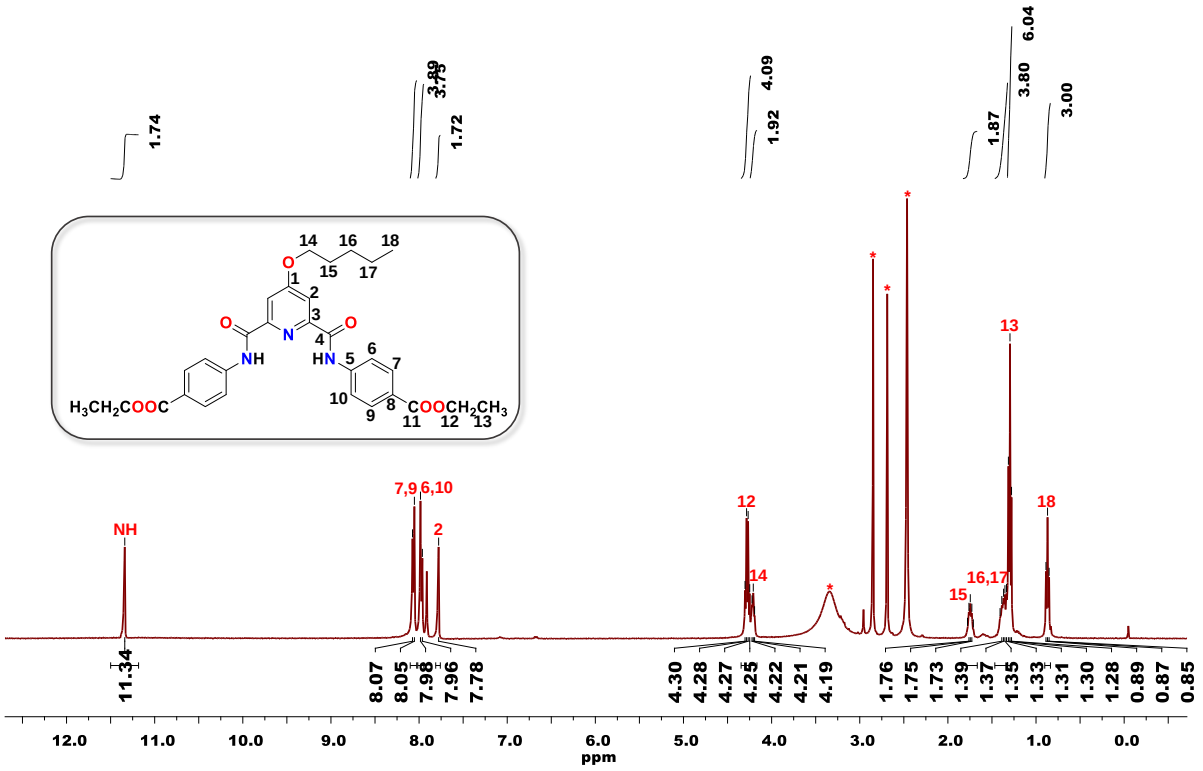

Figure S21. ^{1}H NMR spectrum of **L'''** in DMSO-d_6 solvent where * represents the residual solvent and/or adventitious water peaks.

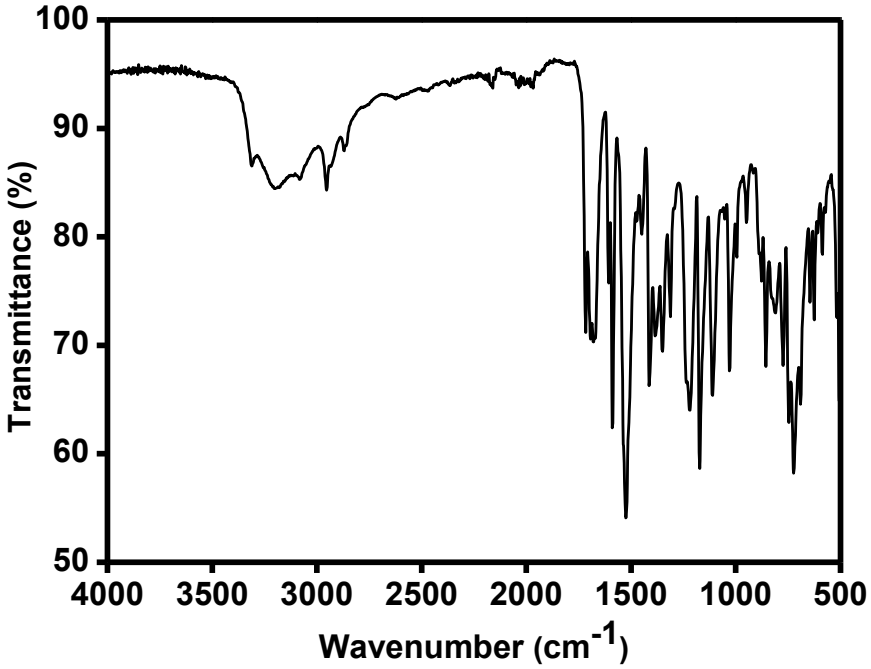

Figure S22. FTIR spectrum of ligand **L2**.

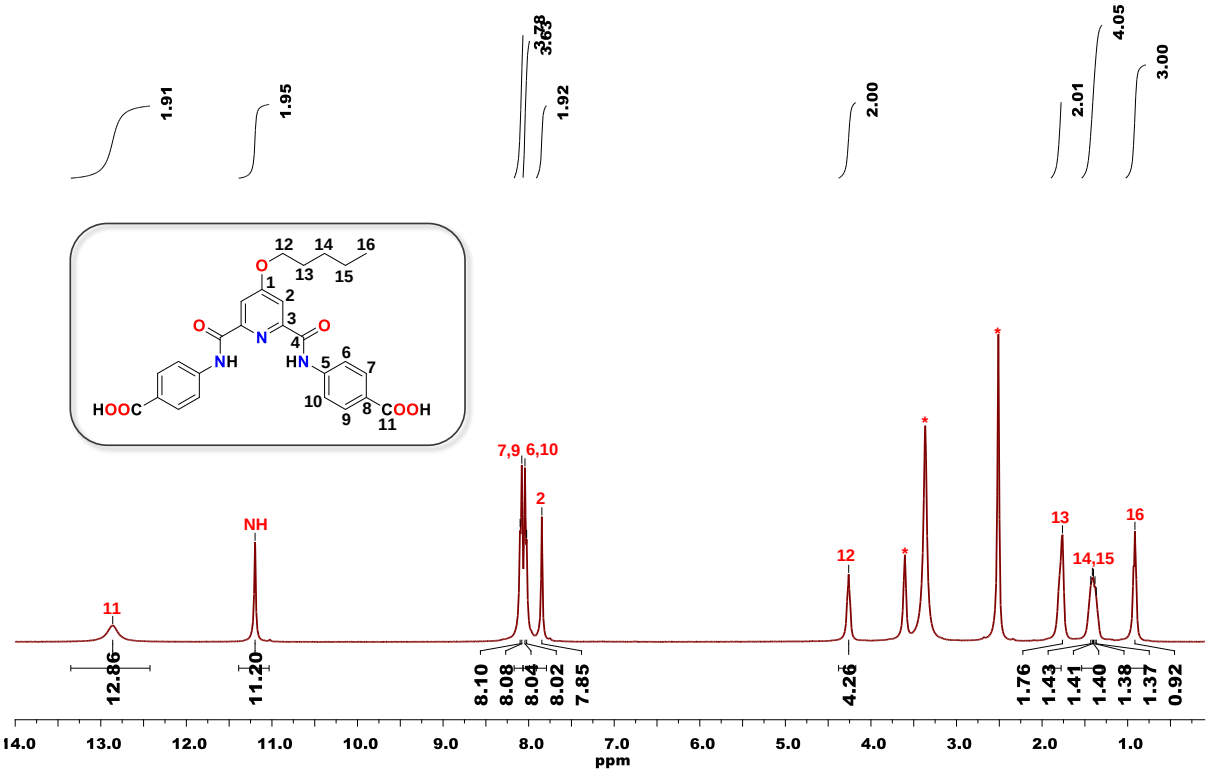

Figure S23. ^{1}H NMR spectrum of ligand **L2** in DMSO-d_6 solvent where * represents the residual solvent and/or adventitious water peaks.

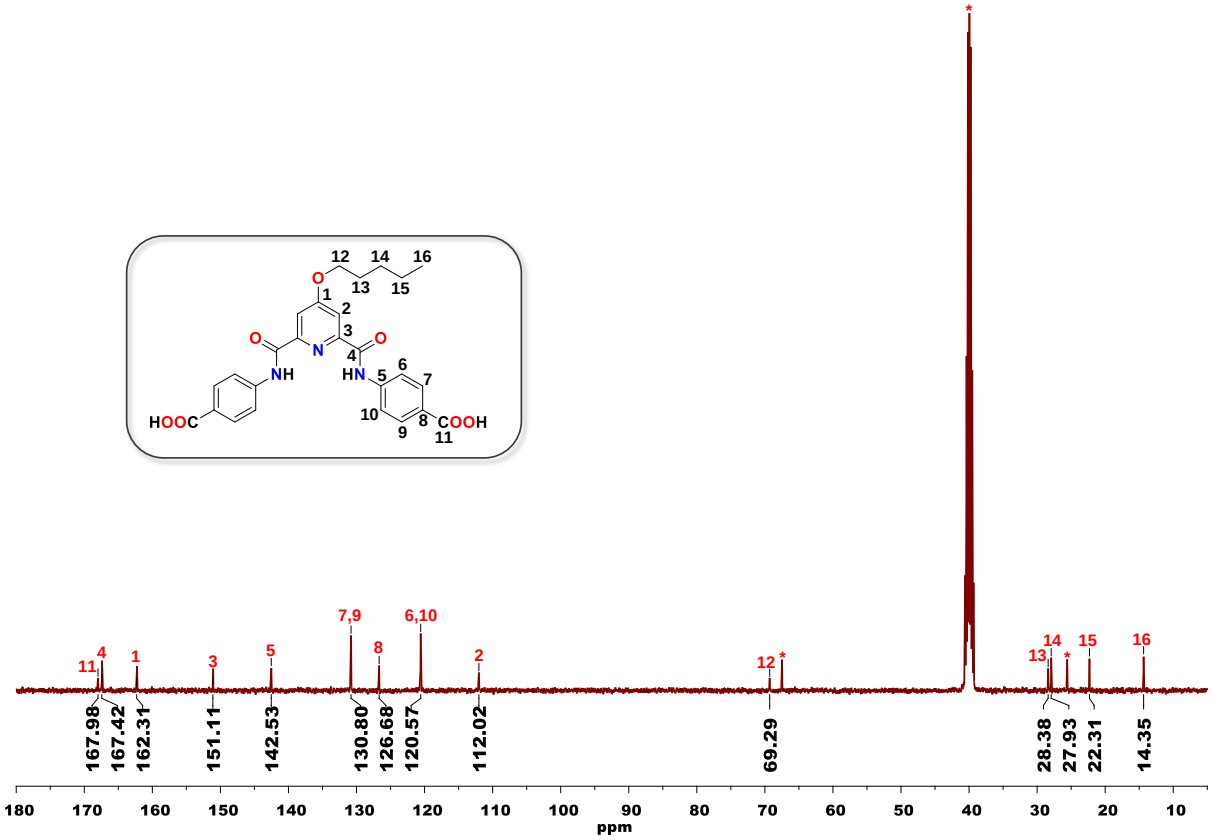

Figure S24. ^{13}C NMR spectrum of ligand **L2** in DMSO-d_6 solvent where * represents the residual solvent peak.

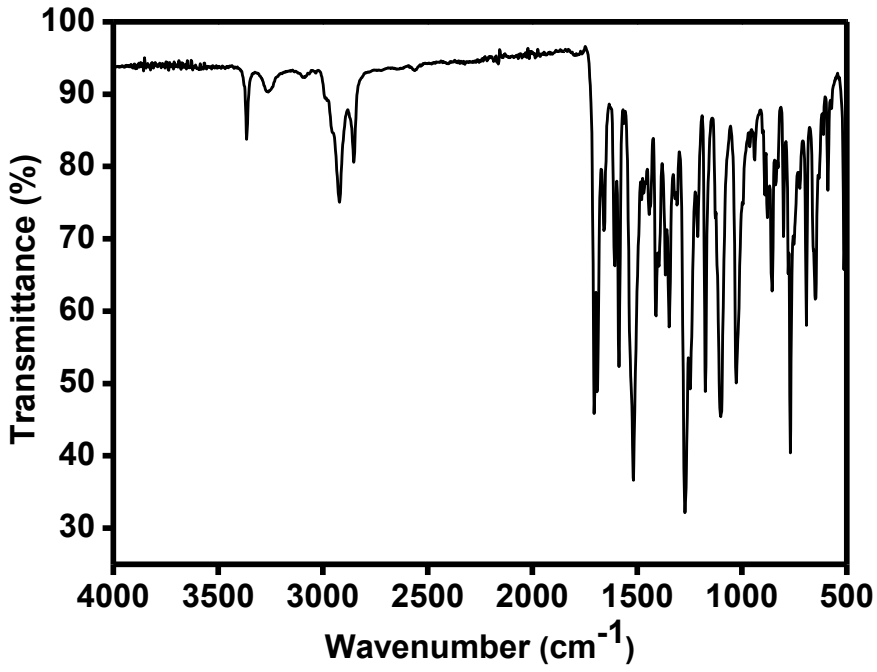

Figure S25. FTIR spectrum of **L''''**.

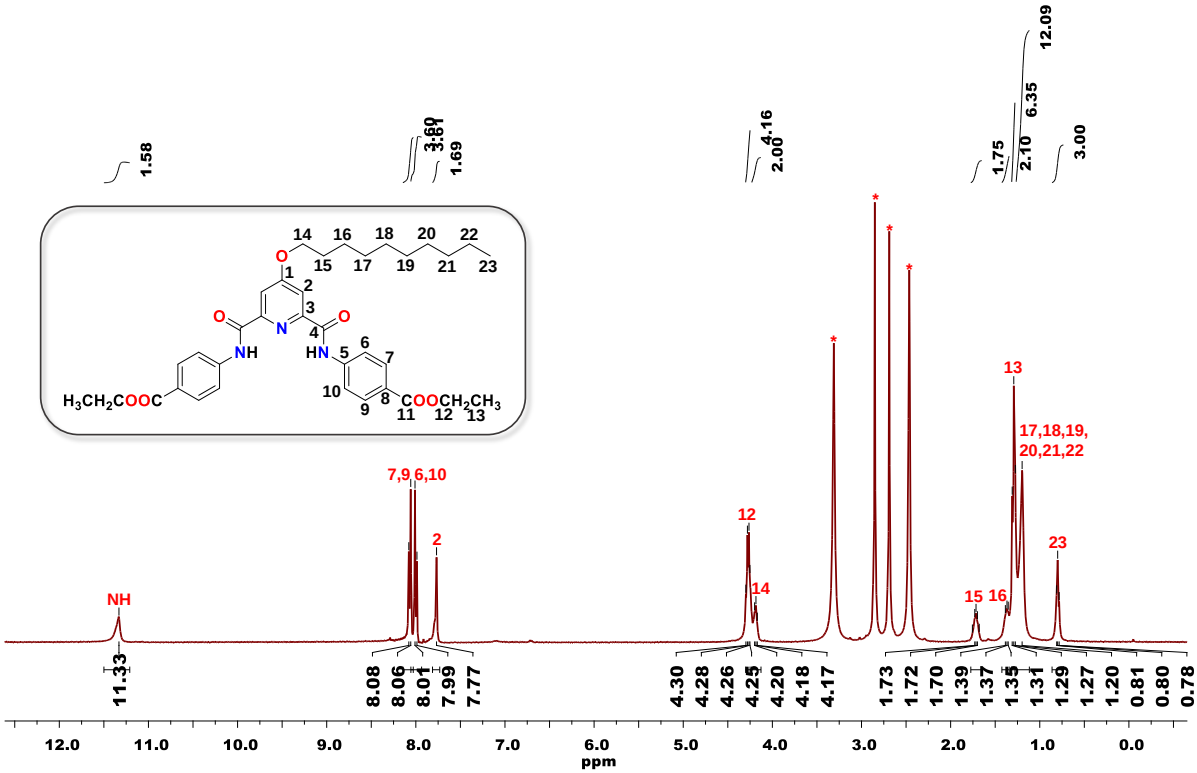

Figure S26. ^{1}H NMR spectrum of **L''''** in DMSO-d_6 solvent where * represents the residual solvent and/or adventitious water peak.

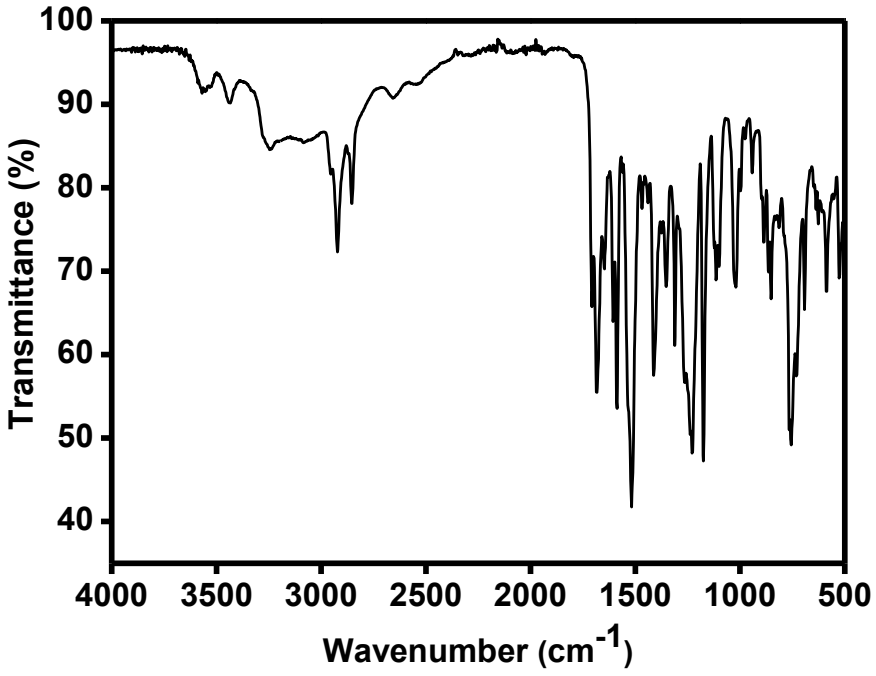

Figure S27. FTIR spectrum of ligand **L3**.

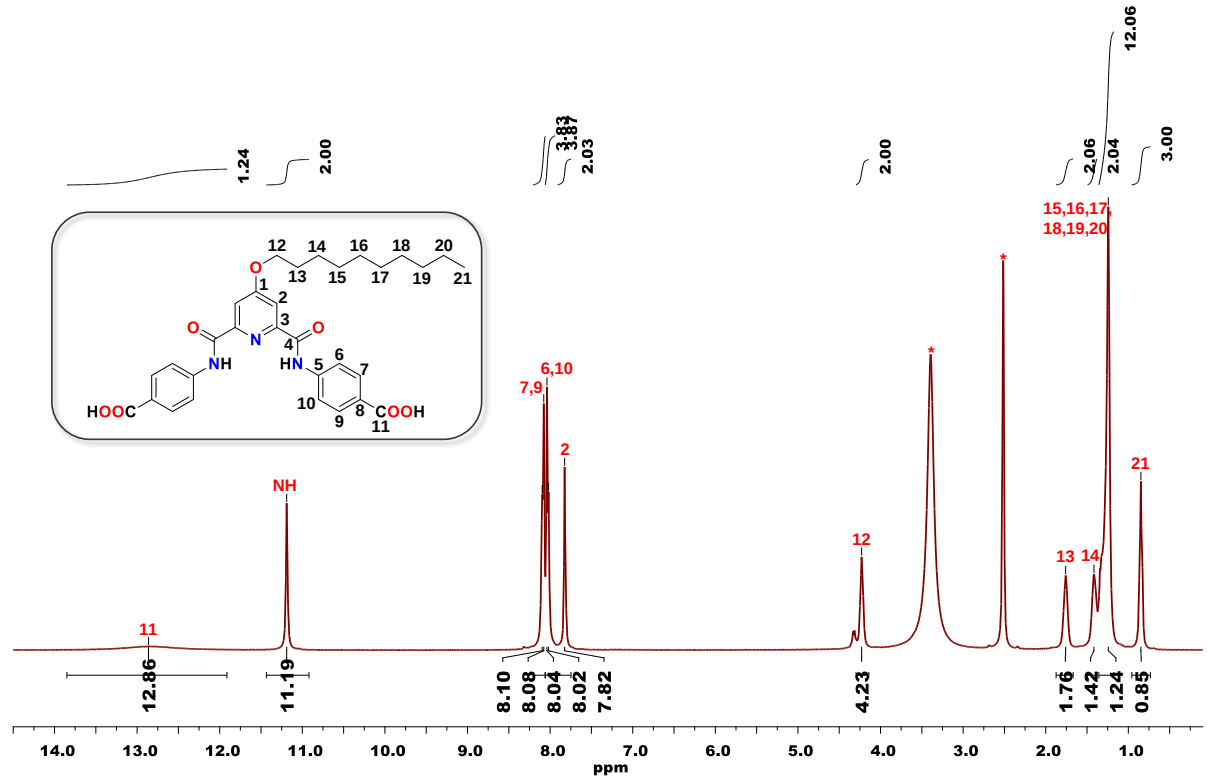

Figure S28. ^{1}H NMR spectrum of ligand **L3** in DMSO-d_6 solvent where * represents the residual solvent and/or adventitious water peak.

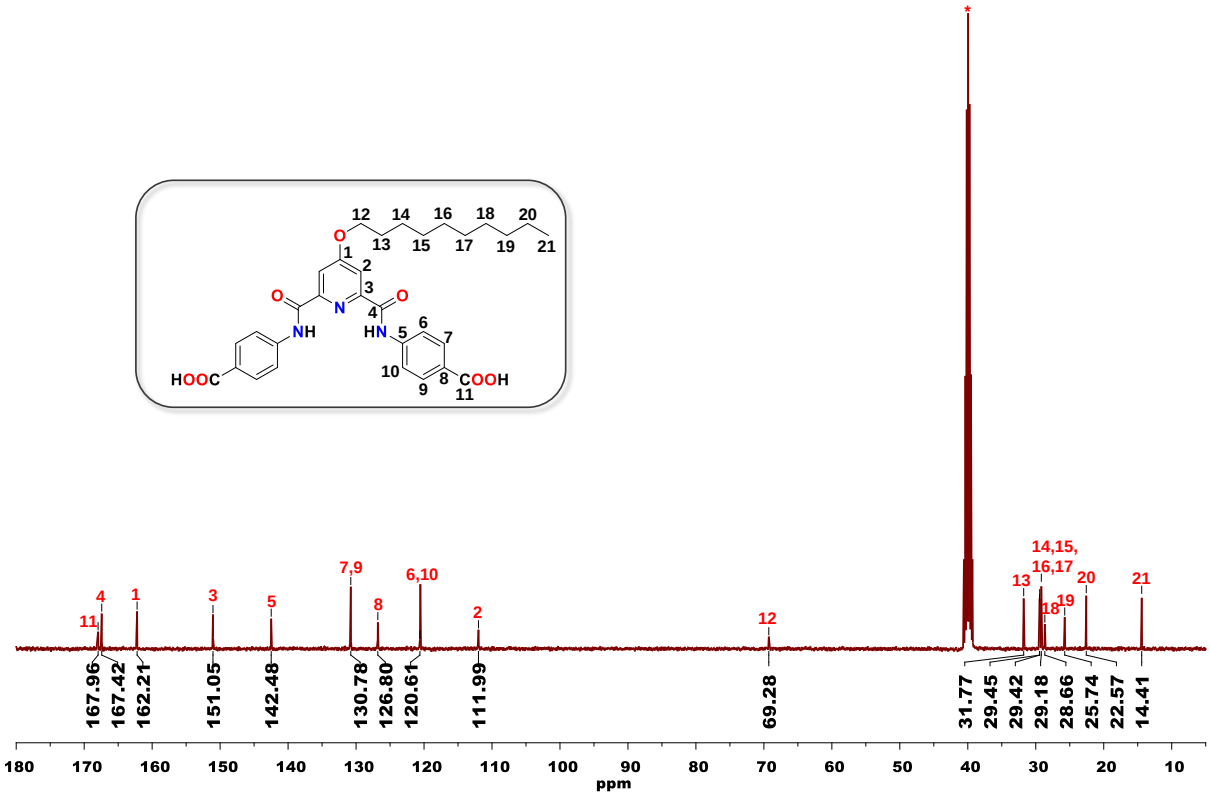

Figure S29. ^{13}C NMR spectrum of ligand **L3** in DMSO-d_6 solvent where * represents the residual solvent peak.

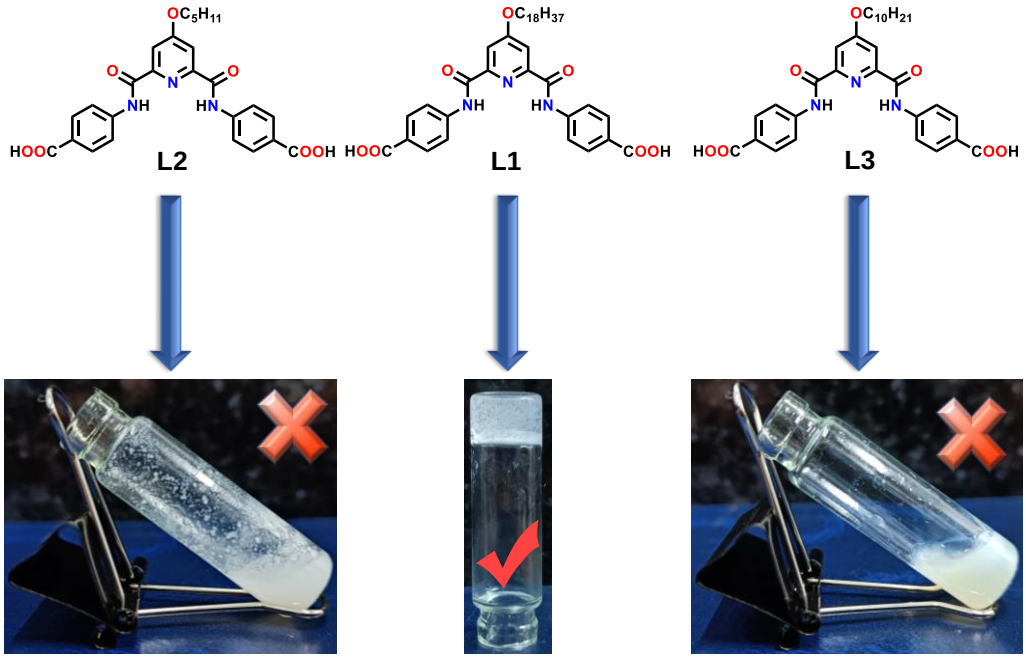

Figure S30. Gelation ability of **L1**, **L2** and **L3** (15 mM) upon addition of a $Ln(OTf)_3$ salt (Ln = Eu(III), Tb(III)).

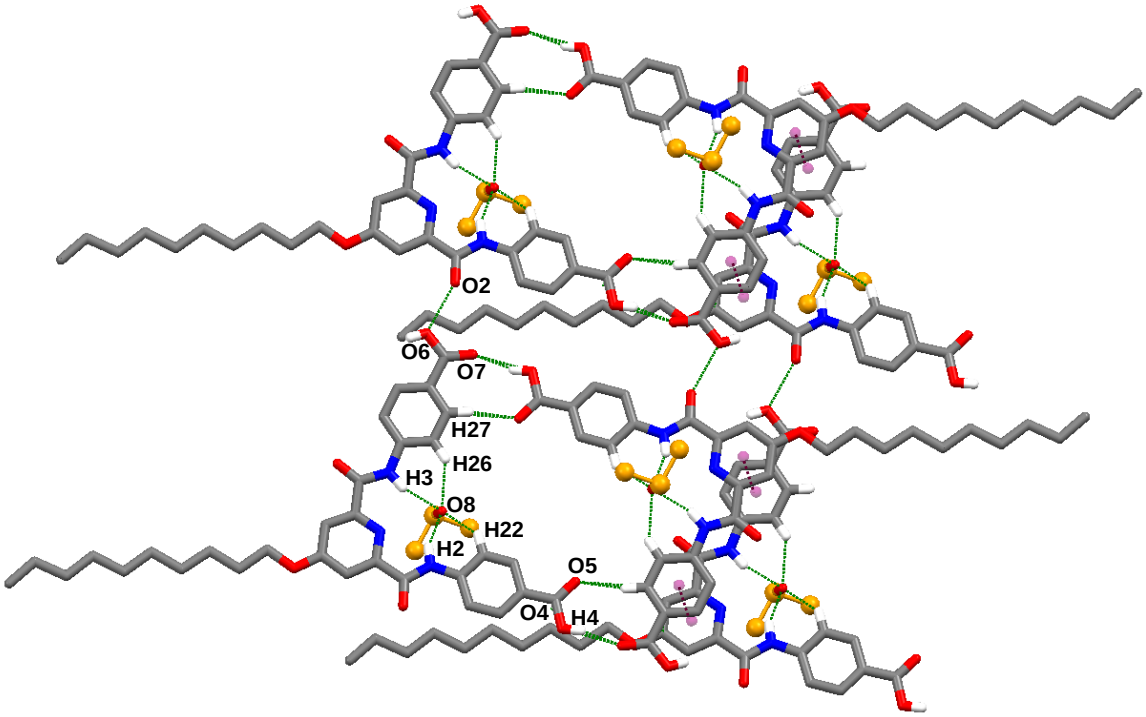

Figure S31. Crystal structure of ligand **L3**, in a view along *a*-axis, showing the packing of different molecules. The lattice DMSO molecule (ball and stick mode where C and O atoms are shown in gold and red, respectively) was found H-bonded within the pincer cavity.

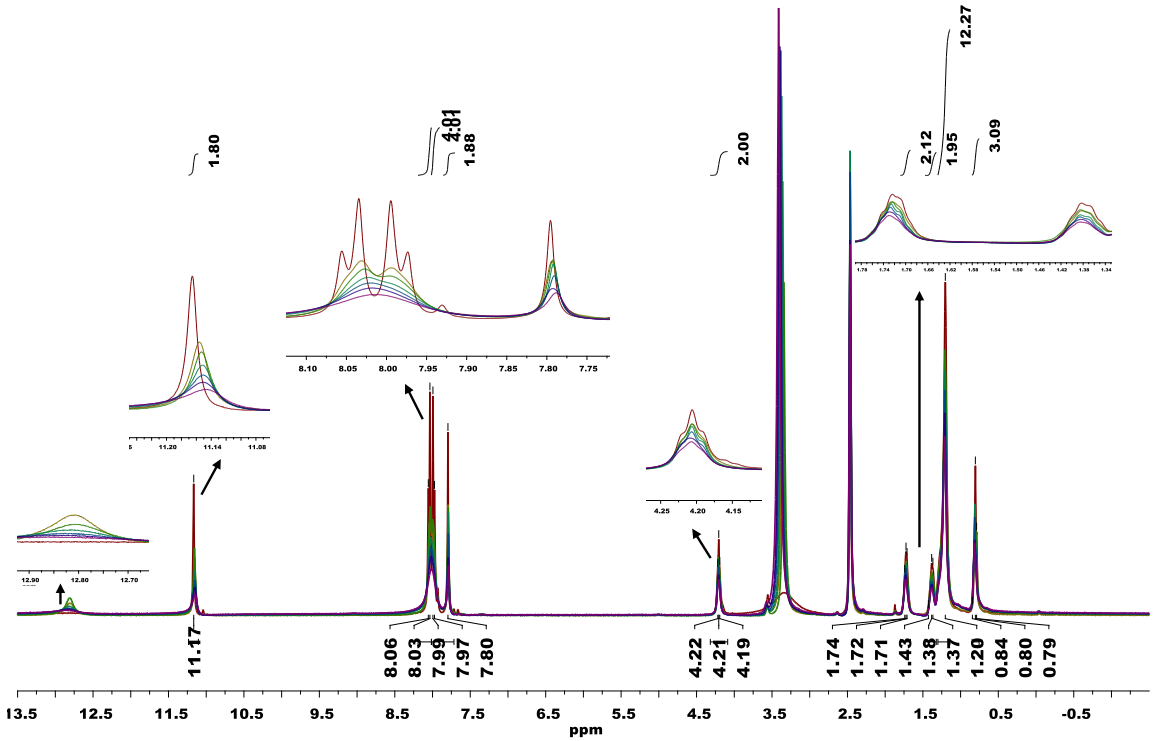

Figure S32. ^{1}H NMR spectral titration of ligand **L3** after the successive addition of up to three equiv. of the Eu^{3+} salt. Spectra were recorded in DMSO-d_6 solvent.

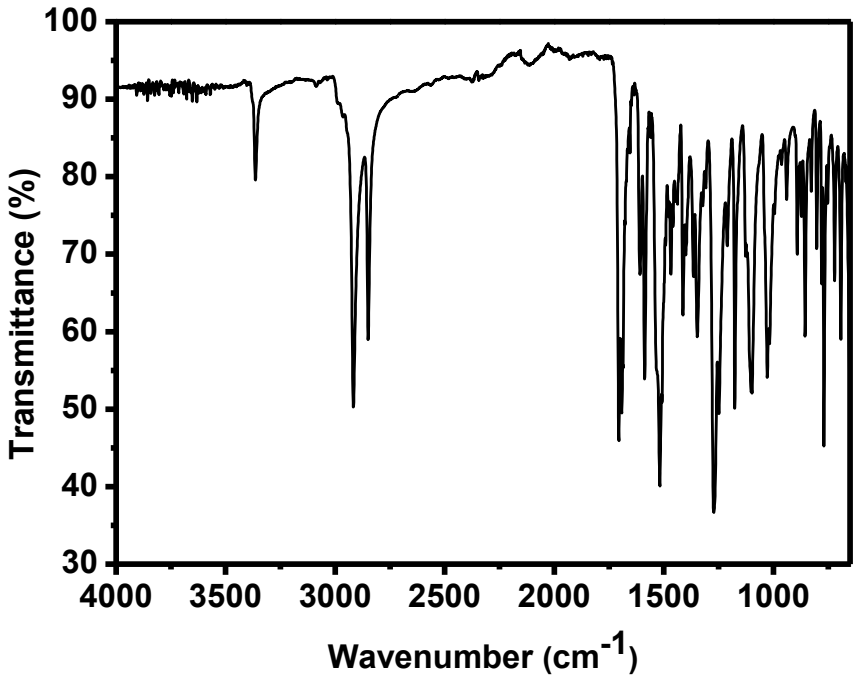

Figure S33. FTIR spectrum of **L''''''**.

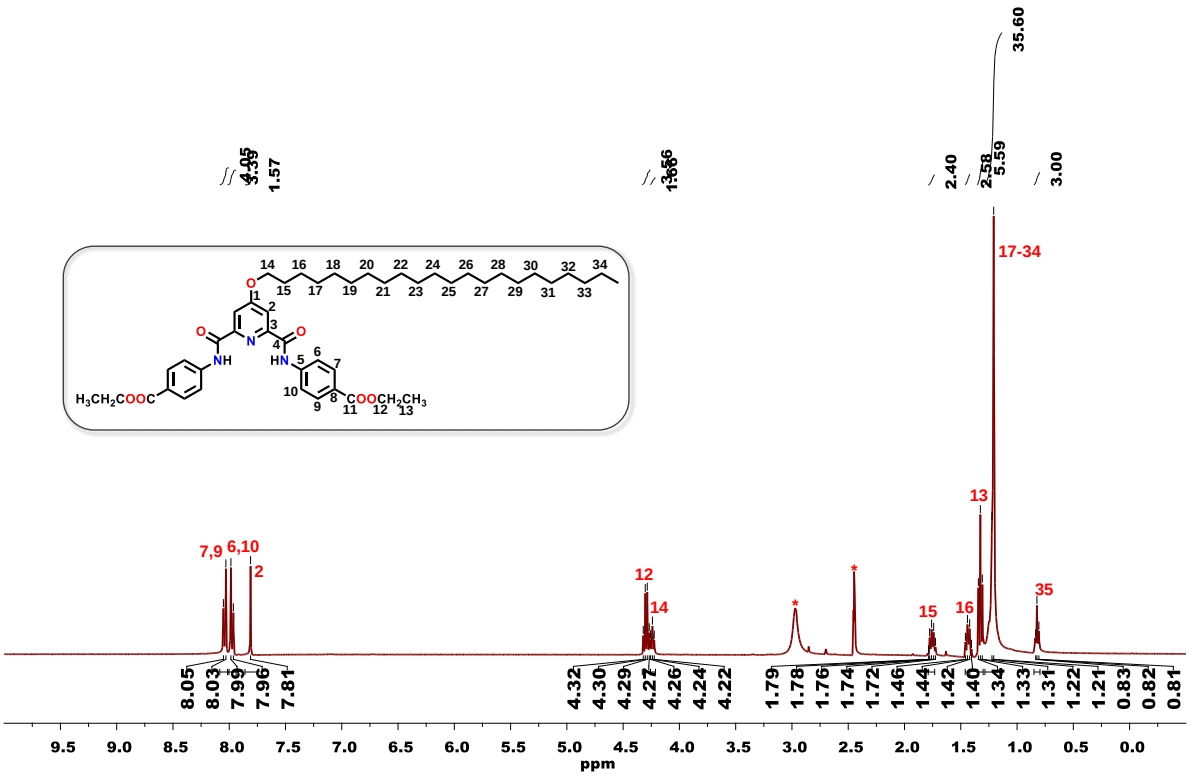

Figure S34. ^{1}H NMR spectrum of **L''''** in DMSO-d_6 solvent where * represents the residual solvent and/or adventitious water peak.

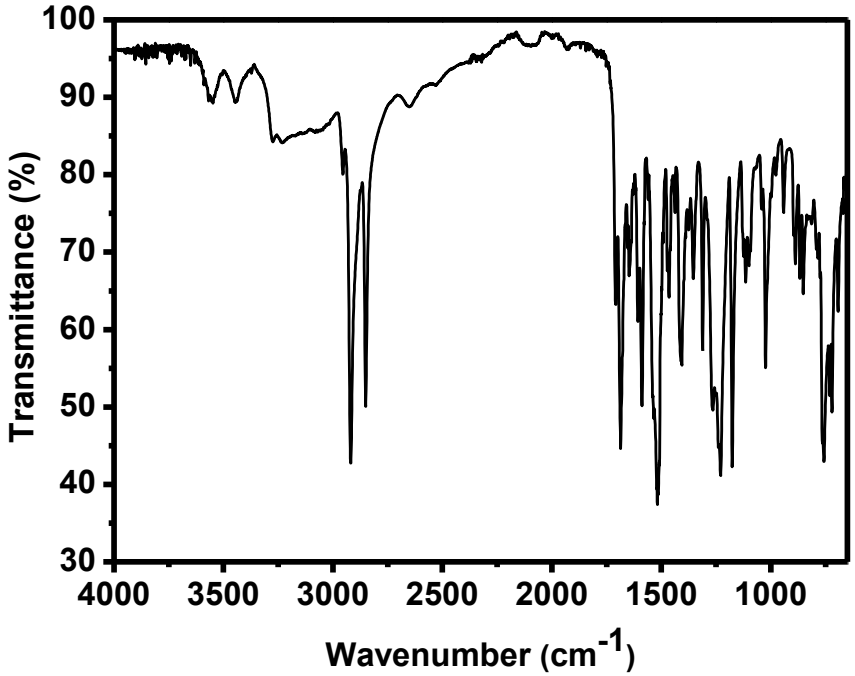

Figure S35. FTIR spectrum of ligand **L4**.

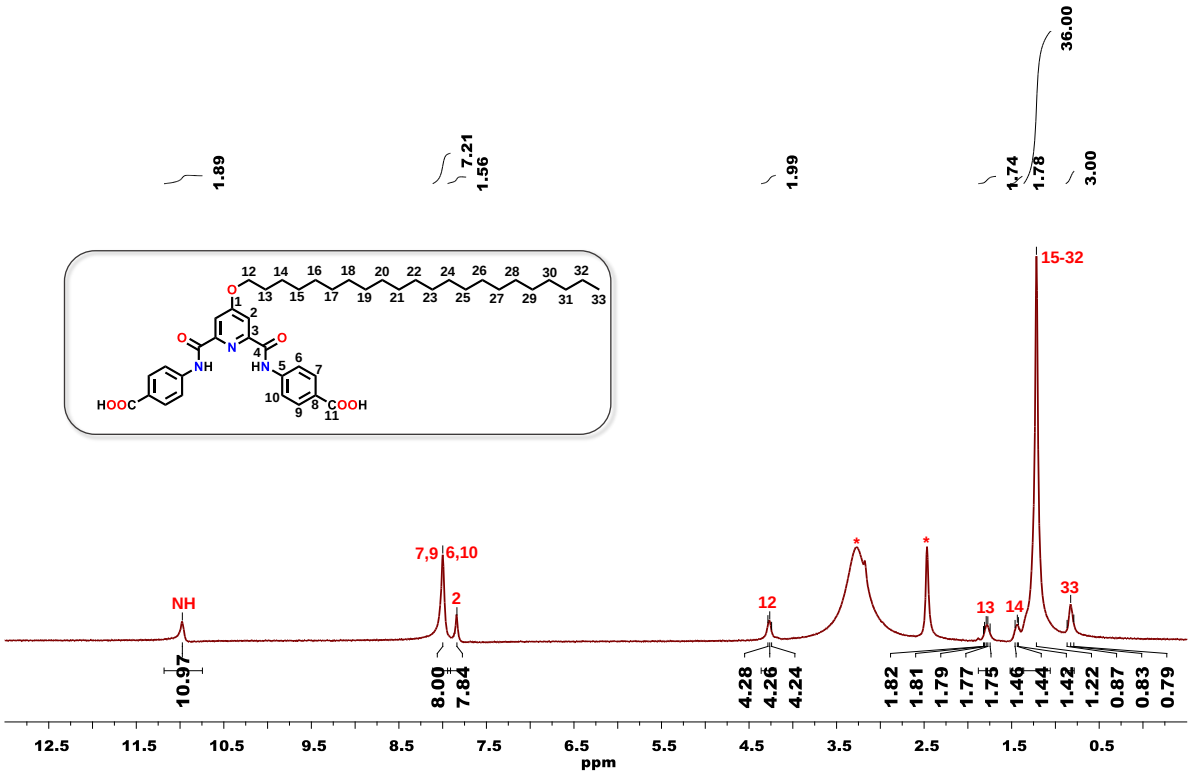

Figure S36. ^{1}H NMR spectrum of ligand **L4** in DMSO-d_6 solvent where * represents the residual solvent and/or adventitious water peak.

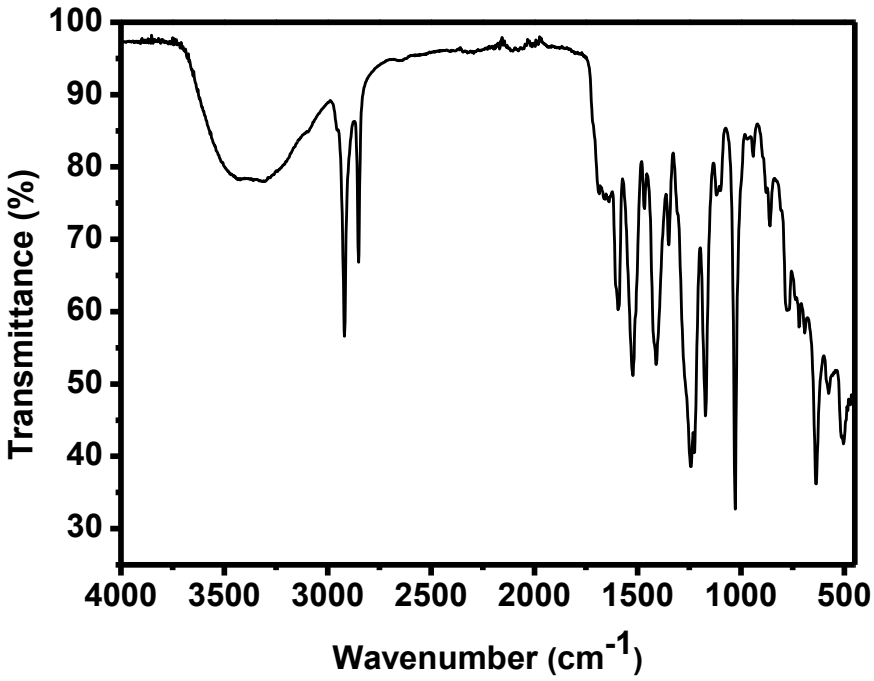

Figure S37. FTIR spectrum of **L4-Eu**.

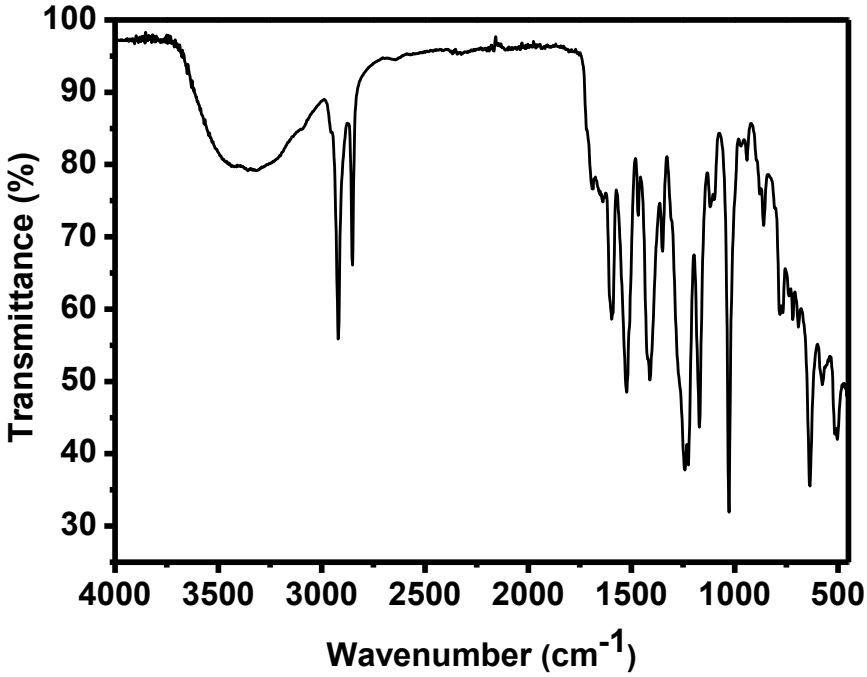

Figure S38. FTIR spectrum of **L4-Tb**.

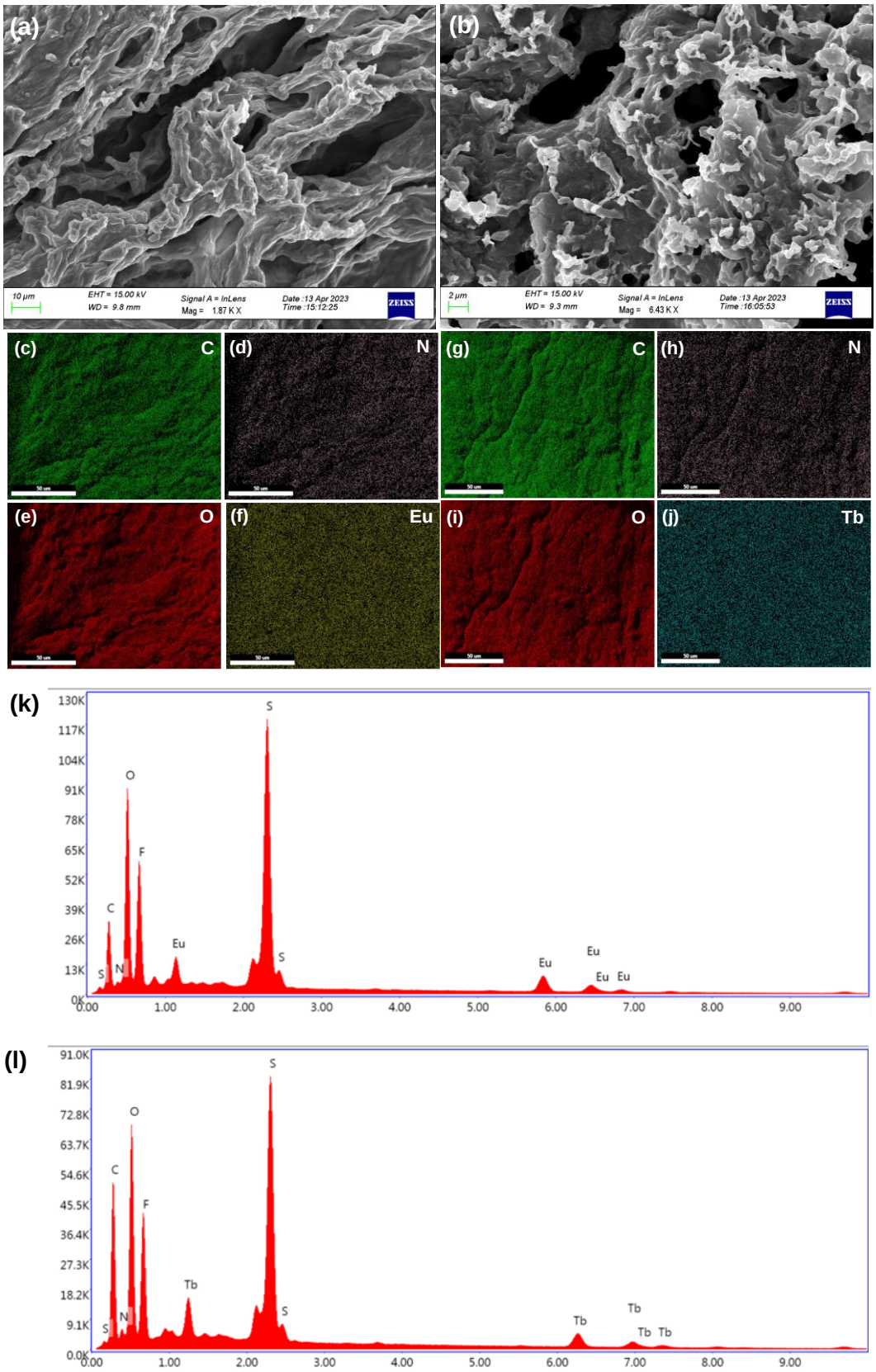

Figure S39. FESEM images of (a) **L4-Eu**, and (b) **L4-Tb**. Elemental mapping analysis of (c-f) **L4-Eu**, and (g-j) **L4-Tb**. EDAX spectra for (k) **L4-Eu** and (l) **L4-Tb**.

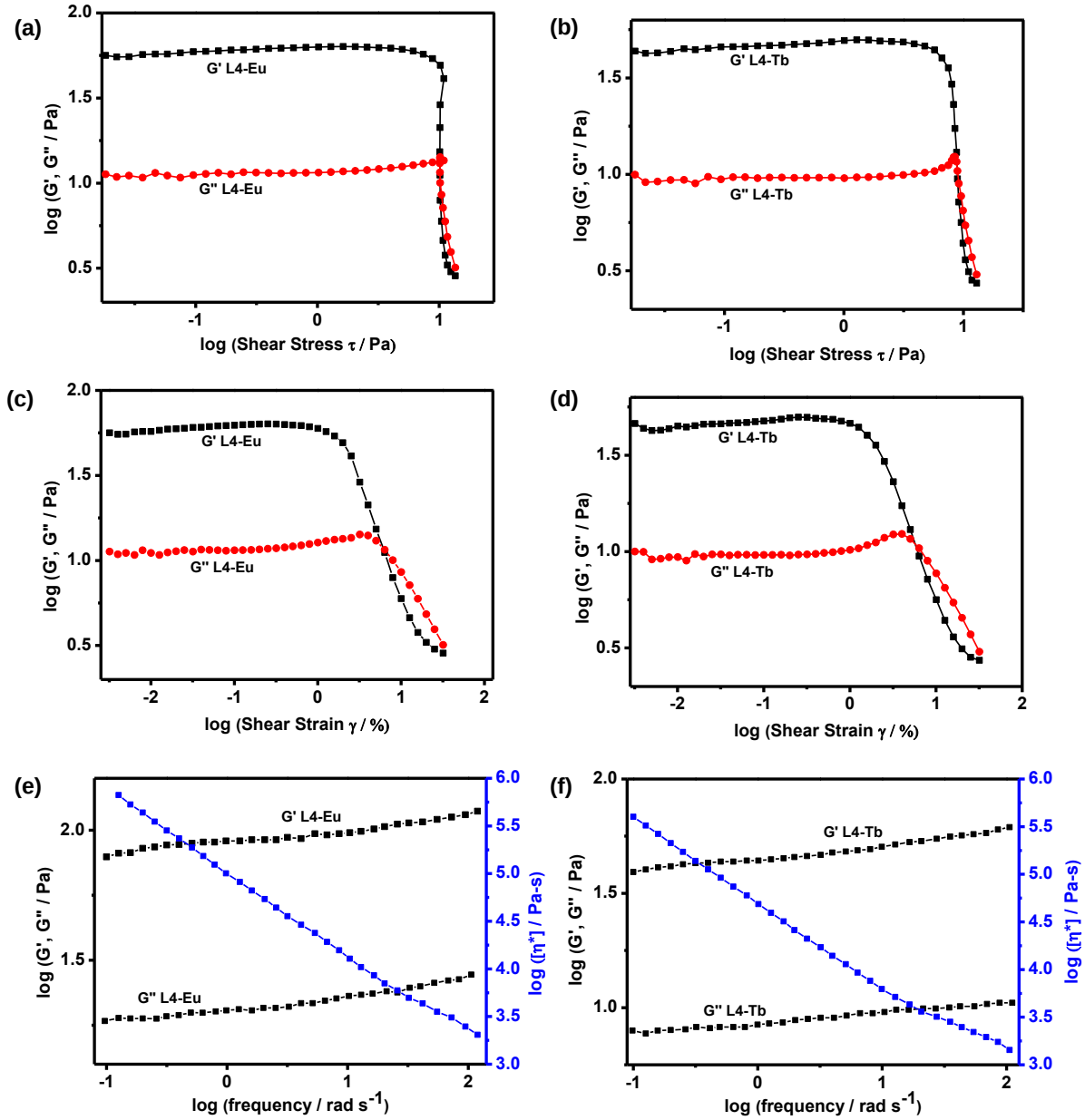

Figure S40. Rheological measurements for **L4-Eu** and **L4-Tb**. Dynamic stress sweep at constant frequency for (a) **L4-Eu** and (b) **L4-Tb**. Dynamic strain sweep at constant frequency for (c) **L4-Eu** and (d) **L4-Tb**. Dynamic frequency sweep at constant strain and secondary axis showing the complex viscosity for (e) **L4-Eu** and (f) **L4-Tb**.

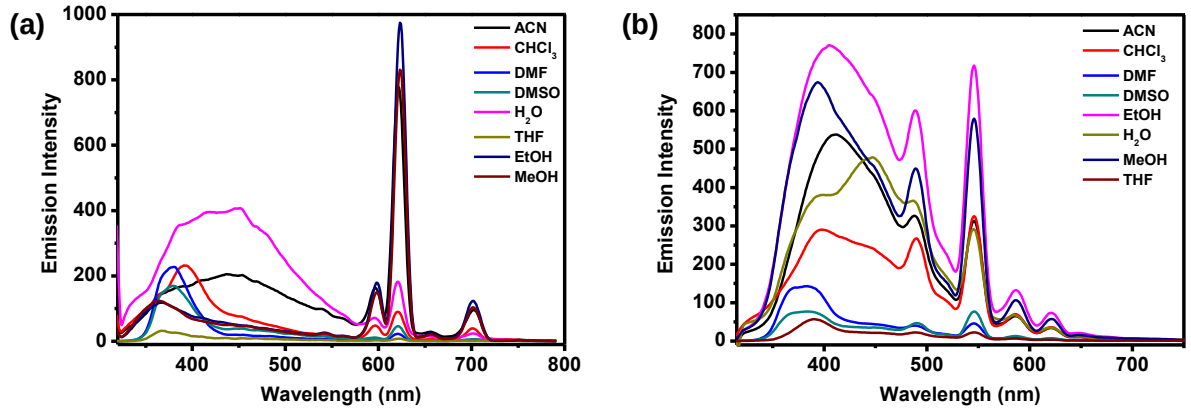

Figure S41. Emission spectra of (a) **L1-Eu** and (b) **L1-Tb** recorded in different solvents.

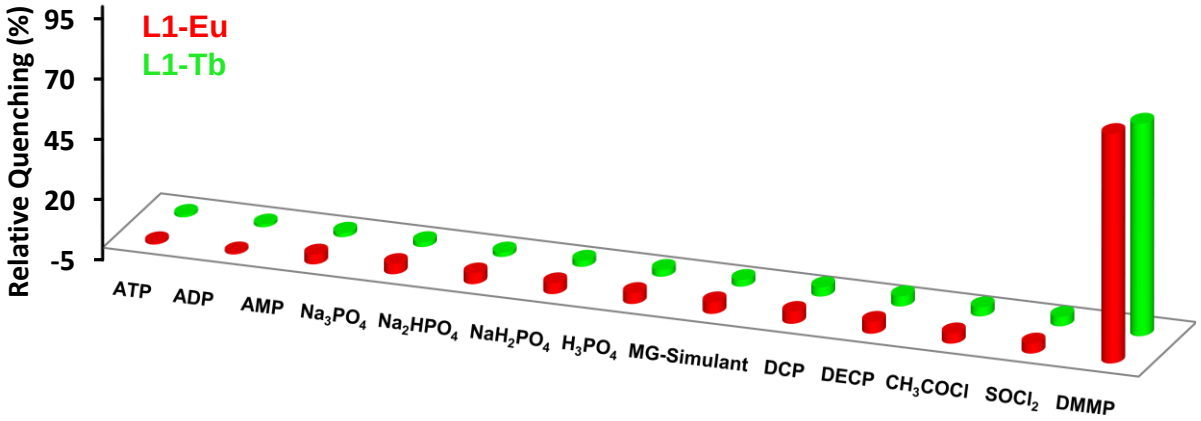

Figure S42. Bar diagram showing relative quenching in the emission intensity of **L1-Eu** (red pillars) and **L1-Tb** (green pillars) in the presence of assorted analytes (50 μM).

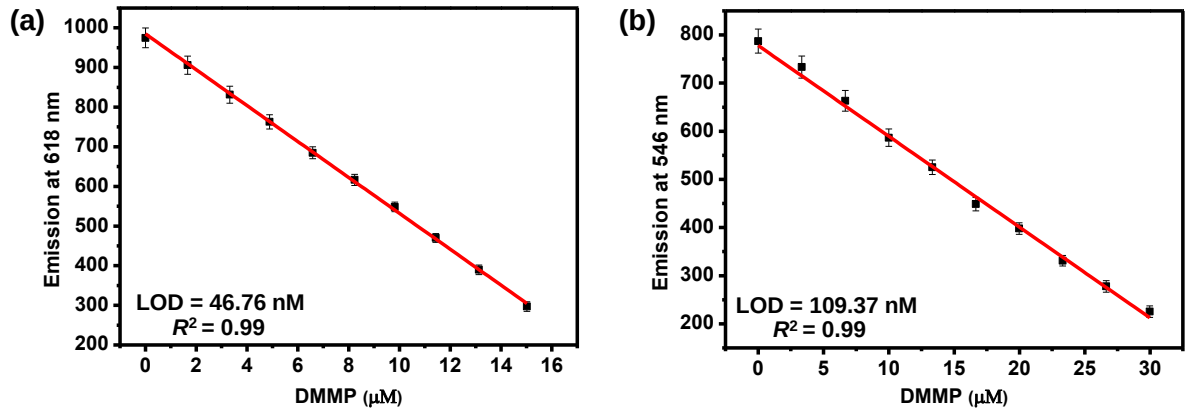

Figure S43. Determination of detection limits for DMMP by (a) **L1-Eu** and (b) **L1-Tb** from the emission spectral titrations.

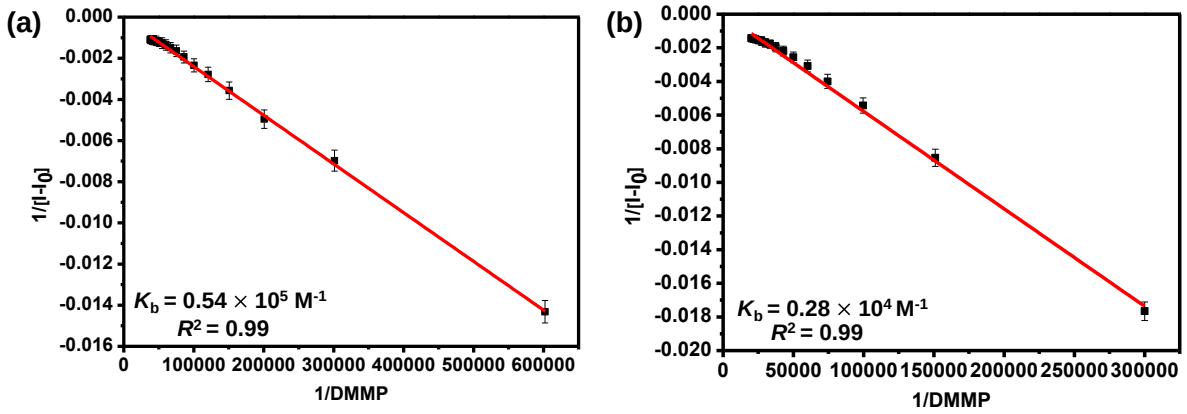

Figure S44. Determination of binding constants by Benesi-Hildebrand plots for the detection of DMMP by (a) **L1-Eu** and (b) **L1-Tb** from the emission spectral titrations.

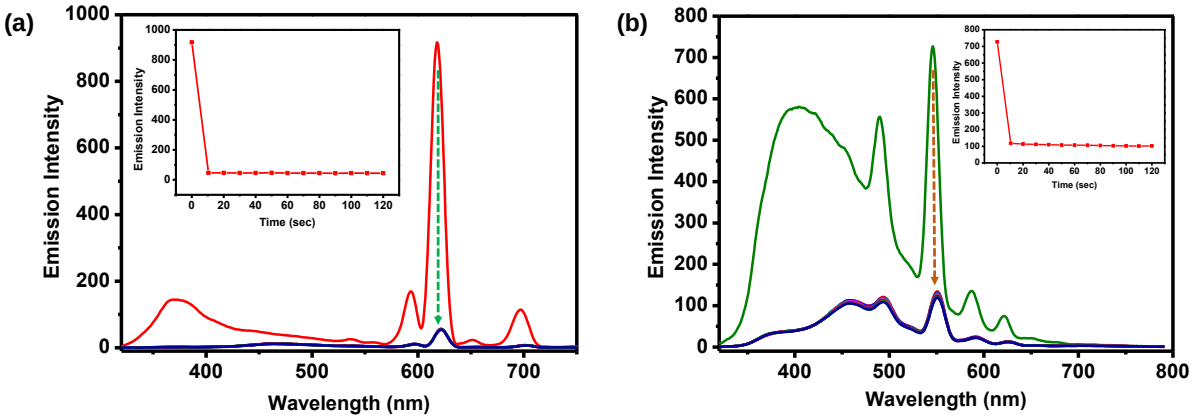

Figure S45. Change in the emission spectra of (a) **L1-Eu** and (b) **L1-Tb** as a function of time in the presence of DMMP (50 μM). Both insets, respectively, show the response time of (a) **L1-Eu** and (b) **L1-Tb** for the detection of DMMP.

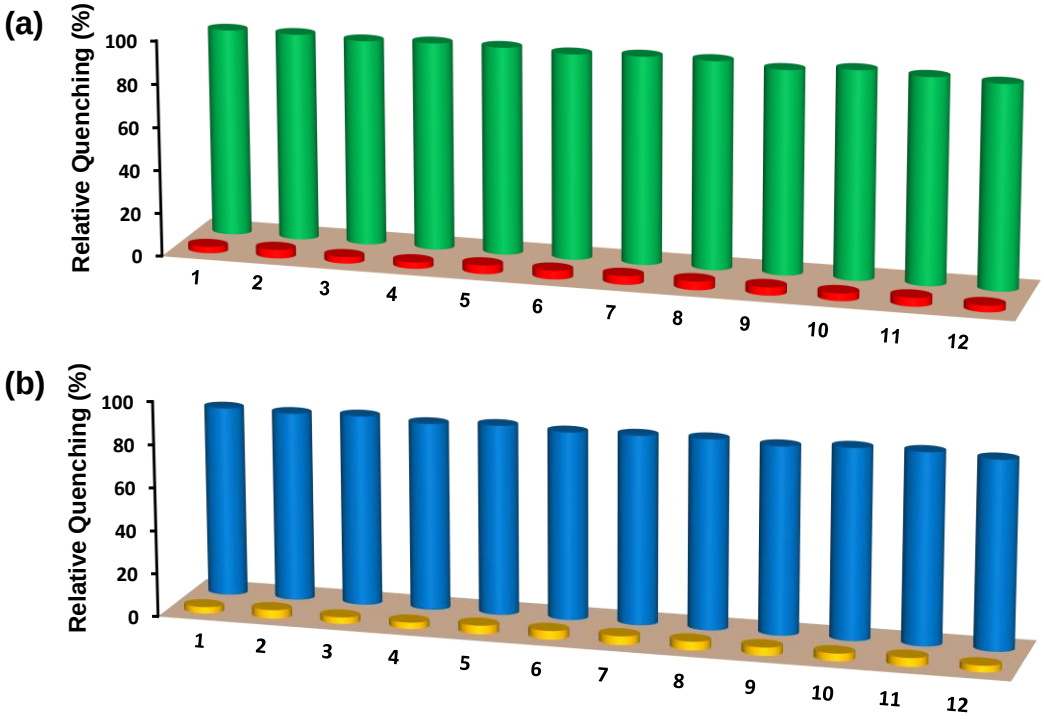

Figure S46. (a) Selectivity of **L1-Eu** towards DMMP in the presence of other analytes: **L1-Eu** + analytes (red pillars) and **L1-Eu** + analytes + DMMP (green pillars). (b) Selectivity of **L1-Tb** toward DMMP in the presence of other analytes: **L1-Tb** + analytes (yellow pillars) and **L1-Tb** + analytes + DMMP (blue pillars) (1: ATP, 2: ADP, 3: AMP, 4: Na_3PO_4, 5: Na_2HPO_4, 6: NaH_2PO_4, 7: H_3PO_4, 8: MG-Simulant, 9: DCP, 10: DECP, 11: CH_3COCl, 12: $SOCl_2$). All studies were performed in EtOH.

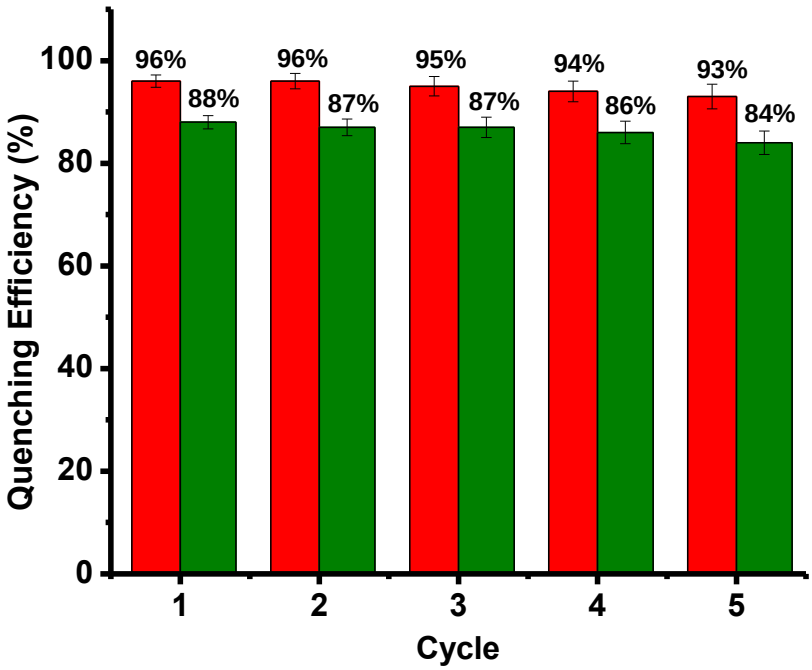

Figure S47. A bar graph displaying the reusability of **L1-Eu** (red bar) and **L1-Tb** (green bar) for the sensing of DMMP for five consecutive cycles.

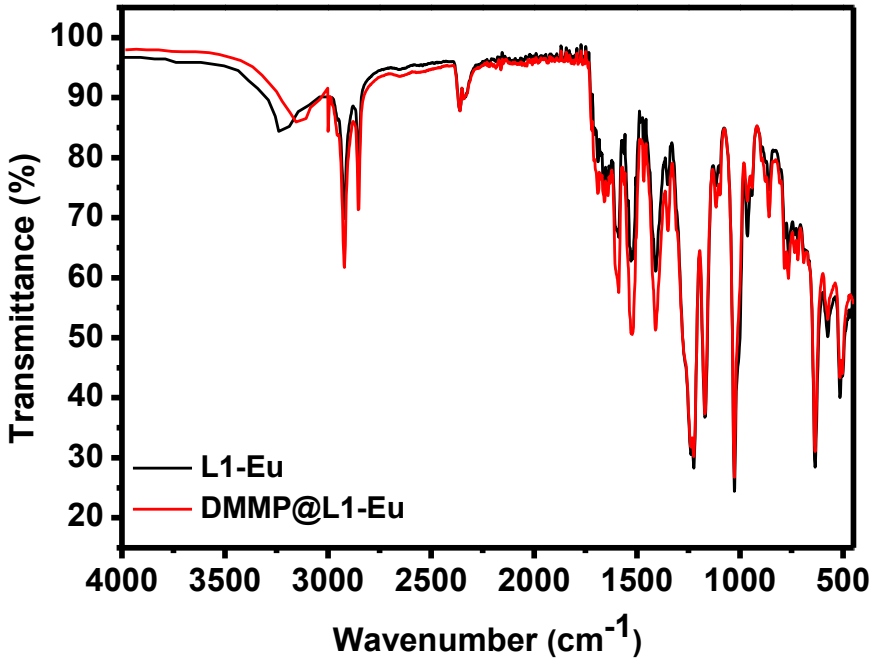

Figure S48. FTIR spectra of **L1-Eu** (black trace) and DMMP@**L1-Eu** (red trace).

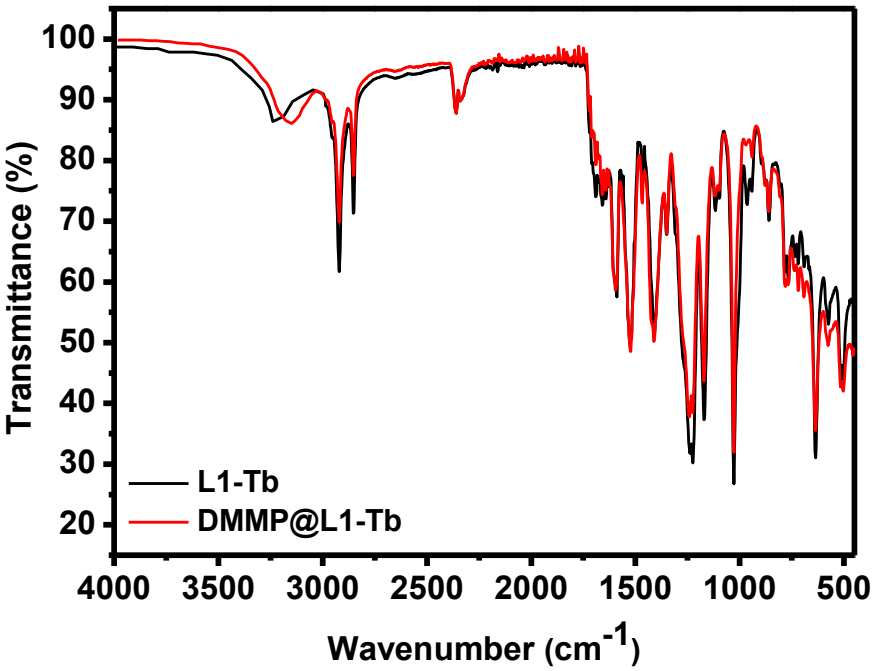

Figure S49. FTIR spectra of **L1-Tb** (black trace) and DMMP@**L1-Tb** (red trace).

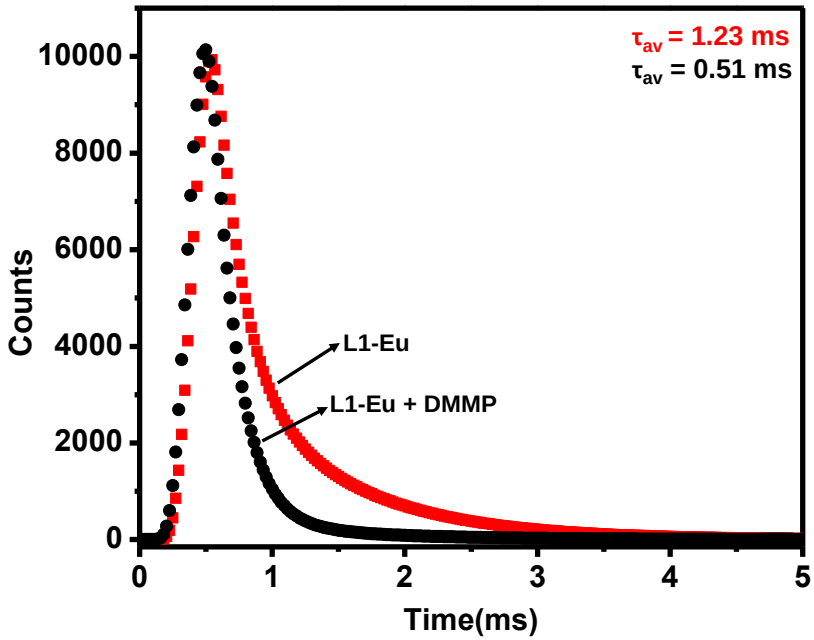

Figure S50. Lifetime profile of **L1-Eu** in the absence and presence of DMMP in EtOH (λ_{ex} = 300 nm).